Bucher *et al. Swiss J Geosci* (2020) 113:1
https://doi.org/10.1186/s00015-020-00354-6

SGG SGS sc | nat
Swiss Journal of Geosciences

ORIGINAL PAPER Open Access

The Theodul Glacier Unit, a slab of pre-Alpine rocks in the Alpine meta-ophiolite of Zermatt-Saas, Western Alps

Kurt Bucher[1*], Tobias Björn Weisenberger[2], Sebastian Weber[3], Oliver Klemm[4] and Fernando Corfu[5]

Abstract

The Theodul-Glacier-Unit (TGU) is a 100 m thick and 2 km long slab of pre-Alpine schist, gneiss and mafic rocks tectonically emplaced in the eclogite-facies Zermatt-Saas meta-ophiolite nappe (ZSU). The meta-sedimentary rocks occur mostly as garnet-phengite schists with locally cm-sized garnet porphyroblasts. The metavolcanic basic rocks are present as variably retrogressed eclogites showing a continental basalt signature and contain abundant zircon, which is unusual for basalts. The zircons dated with the U–Pb system yield an upper intercept age of 295 ± 16 Ma and a lower intercept age of 145 ± 34 Ma. The early Permian age is interpreted to represent the age of high-grade granulite facies metamorphism, evidence of which is also preserved in the cores of garnet porphyroblasts of the Grt-Ph schists. The lower intercept age corresponds to the time of continental breakup and the initiation of the Tethys in the Mid-Jurassic; these events may have created the TGU as an extensional allochton. Eclogite facies metamorphism recorded by the TGU rocks occurred during Alpine subduction at 57 Ma, the Lu–Hf age of TGU eclogite garnets. The TGU reached a depth of about 53 km at *P–T* conditions of 1.7 GPa and 520 °C derived from both, eclogite and Grt-Ph schist. This is in contrast to the ZSU surrounding the TGU with a reported subduction depth of more than 80 km at 43 Ma. It is proposed here that TGU and ZSU were subducted separately out of sequence. After juxtaposition of the two units during late Alpine thrusting and folding forming the present day geometry of nappes in the Zermatt-Saas region both units were progressively metamorphosed to about 650 MPa and 470 °C. This late prograde metamorphism at 34 Ma produced oligoclase + magnesio-hornblende in the matrix of Grt-Ph schists and eclogites. The derived TGU data document a complete Wilson Cycle.

Keywords: Theodul-Glacier-Unit, Granulite, Eclogite, Permian zircon, Ophiolite, Zermatt-Saas Unit

1 Introduction

The very rapidly retreating Upper Theodul Glacier south of Zermatt close to the Swiss-Italian border exposed a slab of strikingly rusty-weathering rocks in the metamorphic Mesozoic ophiolite of the Zermatt-Saas Unit (ZSU) close to the major thrust contact to the cover unit, the Combin Unit, above (Figs. 1 and 2). This about 2 × 0.1 km large slab is made up of rocks that are not typical of the ZSU (Weber and Bucher 2015). The slab represents an exotic tectonically emplaced fragment of continental rocks and has been labeled Theodul Glacier Unit (TGU) (Weber and Bucher 2015). The rock assemblage of the TGU is unique to the Zermatt region and the origin and significance of the TGU is scarcely known.

This paper presents new data from eclogite and garnet-phengite schist of the TGU, including zircon ages from the eclogite. The data show that the TGU rocks have been metamorphosed under granulite facies conditions in the Permian. The continental breakup and the initiation of the Tethys in the Mid-Jurassic (Dogger) are reflected by the composition of the zircons. This event created the TGU as an extensional allochton. Alpine subduction

Editorial handling: E. Gnos.

*Correspondence: bucher@uni-freiburg.de
[1] Mineralogy & Petrology, University of Freiburg, Albertstr. 23b, 79104 Freiburg, Germany
Full list of author information is available at the end of the article

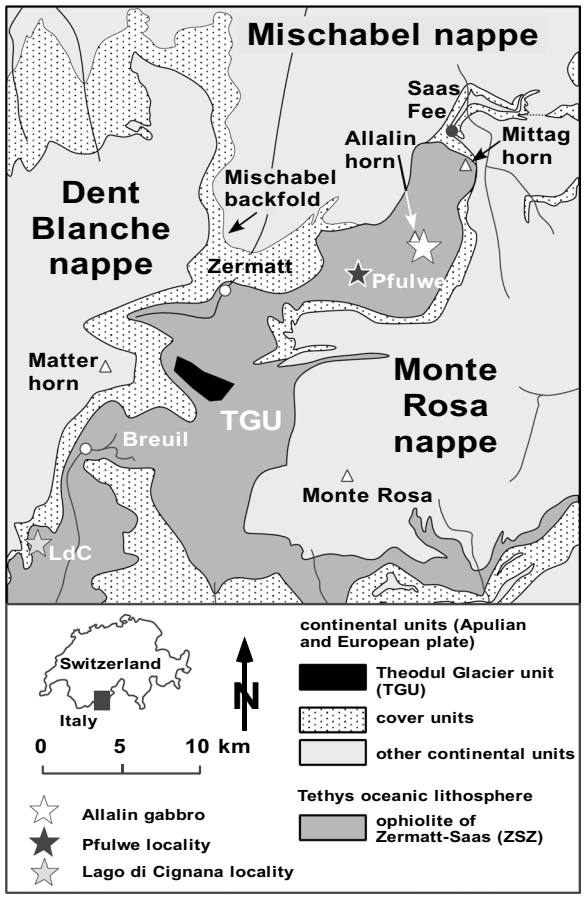

Fig. 1 Simplified tectonic map of the Zermatt-Saas ophiolite zone (modified after Bearth 1967). The Mischabel and Monte Rosa nappe are Penninic crystalline basement (European plate), the Dent Blanche nappe represents Austroalpine continental basement (Apulian plate). *TGU* Theodul Glacier Unit (Weber and Bucher 2015) see detailed geological map Fig. 3, *LdC* Lago di Cignana coesite locality (Reinecke 1991, 1998), eclogitic pillow lavas at Pfulwe locality (Bucher et al. 2005), eclogite facies meta-gabbro at Allalinhorn (Bucher and Grapes 2009)

and metamorphism generated eclogites from the basic metavolcanic rocks and garnet-phengite schists from the granulites. Together with *P*–*T* models for both rocks, the new zircon data and available Lu–Hf garnet-whole rock analyses (Weber et al. 2015) permit a full reconstruction of the geological history of the TGU and document a complete Wilson Cycle.

2 Regional geology of the zermatt area

The Zermatt region of the Western Alps exposes geological elements from the continental platform of the European plate, the oceanic lithosphere of the former Tethys and continental units of the northern margin of the Apulian ("African") plate (Argand 1908, 1911; Bearth 1967; Handy et al. 2010; Steck et al. 2015). These geological elements are stacked as nappes as a result of the tectonic collision of the plates during the formation of the Alps (e.g. Steck et al. 2015). The Mischabel and Monte Rosa nappe represent European continental material, the Dent Blanche nappe system Apulian continental material (Fig. 1). The geometry of the exposed units is substantially complicated by a large young fold, the Mischabel backfold (e.g. Steck et al. 2015), closing towards south just north of the Zermatt village (Fig. 1).

The Zermatt-Saas meta-ophiolites The material from the former Tethys ocean, known as Zermatt-Saas Unit (ZSU), represents an originally fully developed ophiolite that has experienced metamorphic reworking related first to subduction then to the stacking of the nappes and folding (Bearth 1967; Gosso et al. 1979). The ZSU in the Zermatt region has been subjected to high-pressure and locally ultra-high-pressure metamorphism with pressures reaching 2.4–2.7 GPa at T ~ 600 °C (Bucher et al. 2005; Angiboust et al. 2009; Bucher and Grapes 2009; Groppo et al. 2009; Rebay et al. 2012) during Eocene subduction under the overriding Apulian plate (Bowtell et al. 1994; Rubatto et al. 1998; Lapen et al. 2003; Rubatto and Hermann 2003; Skora et al. 2015).

The oceanic rock assemblage of the ZSU in the Zermatt area consists of: (i) serpentinites representing the hydrated mantle portion of the lithosphere (Li et al. 2004a), (ii) eclogites representing basaltic meta-volcanics, with locally well preserved primary volcanic structures such as pillows (Bearth 1967; Bucher et al. 2005), (iii) various types of eclogite-facies meta-gabbro including ferro-gabbro (Ganguin 1988) and the magnesian Allalin gabbro (Bucher and Grapes 2009) (Fig. 1), and (iv) subordinate amounts of oceanic sediments locally with characteristic Mn-rich quartzites (Bearth and Schwander 1981). The oceanic lithosphere was consumed along an active convergent margin in the south and subducted under the continental lithosphere of the Apulian Plate from Late Cretaceous—Early Tertiary (Rubatto et al. 1998). Portions of the subducted oceanic material were returned to shallower depth along the plate contact (subduction channel) and were subsequently re-deformed and overprinted during continental collision in the Mid-Late Tertiary (Bearth 1967; Barnicoat and Fry 1986; Barnicoat et al. 1995; Steck et al. 2015).

The ophiolites were incorporated in the nappe stack during the late collision phase and form a large N-closing recumbent fold at Mittaghorn near Saas Fee (Fig. 1). European continental basement and its cover units (Monte Rosa and Mischabel nappes) lie structurally below the ophiolites (Fig. 1). The Apulian continental basement (Dent Blanche nappe system, DBN) represents the structurally highest unit overriding all other

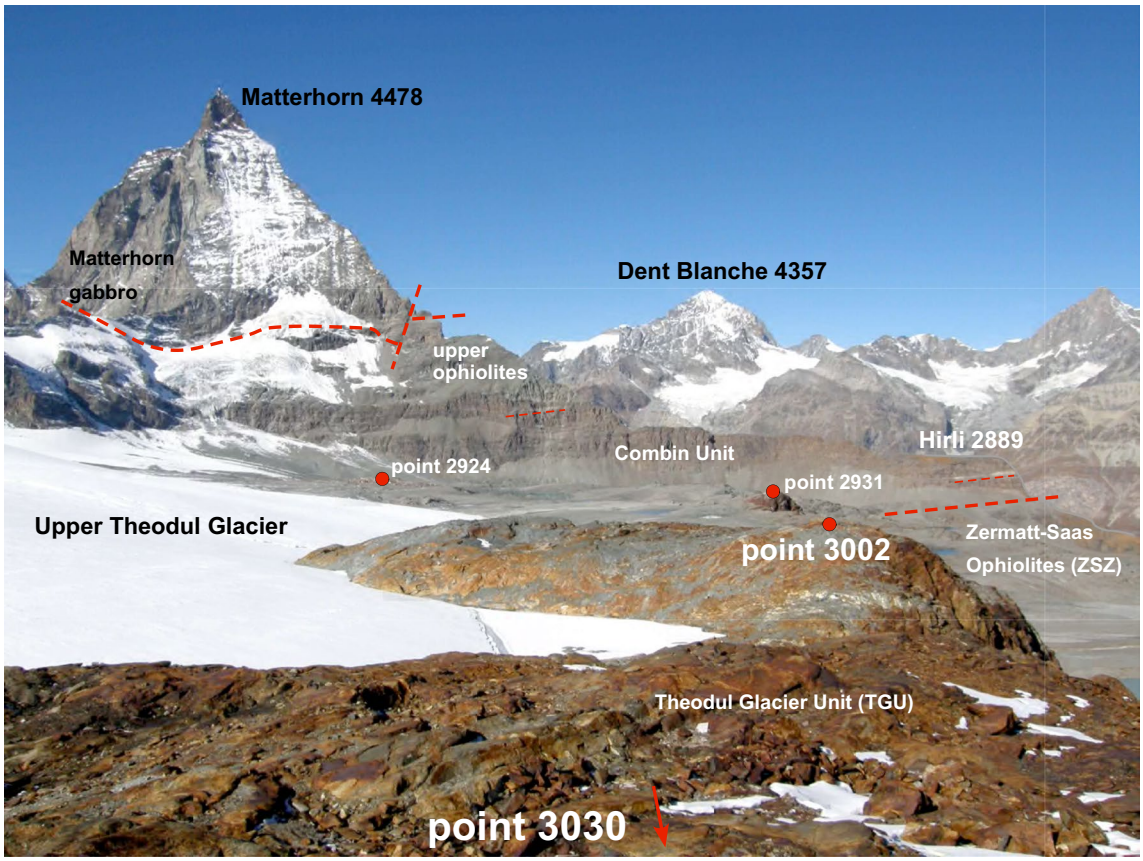

Fig. 2 Overview over the field area as seen from point 3030 to the NW. Matterhorn belongs to the Dent Blanche nappe from the overriding plate (Fig. 1). Below the main Austroalpine thrust follow the upper ophiolites (Tsaté nappe: Escher et al. 1993) and various units hereafter collectively referred to as Combin Unit (Dal Piaz 1965; Bearth 1967). The top of the Zermatt-Saas ophiolite is at the major thrust fault at the foot of Hirli. The rusty-brown weathering garnet-phengite schists and eclogites in the foreground form the Theodul Glacier Unit (TGU) of this study, named after the Upper Theodul Glacier to the south (left) of the outcrops. The topographic points are also shown on the geological map (Fig. 3)

tectonic elements (Figs. 1 and 2). The nappe consists of three major units (Argand 1908; Bucher et al. 2003): (a) the Arolla unit consists of banded granitoid gneisses and massive granites, (b) the Valpelline unit is made of pre-alpine high-grade metamorphic rocks including garnet-cordierite-sillimanite gneiss, tremolite-diopside marble and garnet amphibolite and (c) large masses of Permian gabbro (Dal Piaz et al. 1977; Manzotti et al. 2017, 2018). The Dent Blanche nappe system shows complex internal Alpine deformation (Bucher et al. 2003, 2004) and can be subdivided into various sub-nappes (Dal Piaz et al. 2001; Manzotti et al. 2014; Dal Piaz et al. 2015).

Other regional and local units: The Combin Unit (CU) consists predominantly of Mesozoic meta-sediments and meta-ophiolites, mainly calcareous micaschists and greenschists, but also Triassic marble and quarzite (Bearth and Schwander 1981) (Figs. 1 and 2). It preserves rare blueschist facies assemblages but no eclogites (Bucher et al. 2004). The CU basal thrust (Figs. 1 and 2) is, therefore, a major discontinuity in metamorphic grade and juxtaposes two units with contrasting subduction-exhumation histories during late collision and nappe stacking. The Tsaté nappe with relics of metamorphic ophiolitic material is located between the CU and the DBN (Escher et al. 1993) labeled as upper ophiolites on Fig. 2. The metabasic rocks of the Tsaté nappe do not show eclogite facies assemblages.

Slices of continental rocks comprising also pre-Tethys metasediments occur between ZSU and CU, for instance the Etirol Levaz slice (Ballèvre et al. 1986; Fassmer et al. 2016) south of the Lago di Cignana locality (LdC on Fig. 1).

3 The theodul glacier unit

3.1 Structure

The Theodul Glacier Unit (Fig. 1) is a 100 m thick and 2 km long slab of schist, gneiss and eclogite (Figs. 2, 3 and 4) within the uppermost portion of the

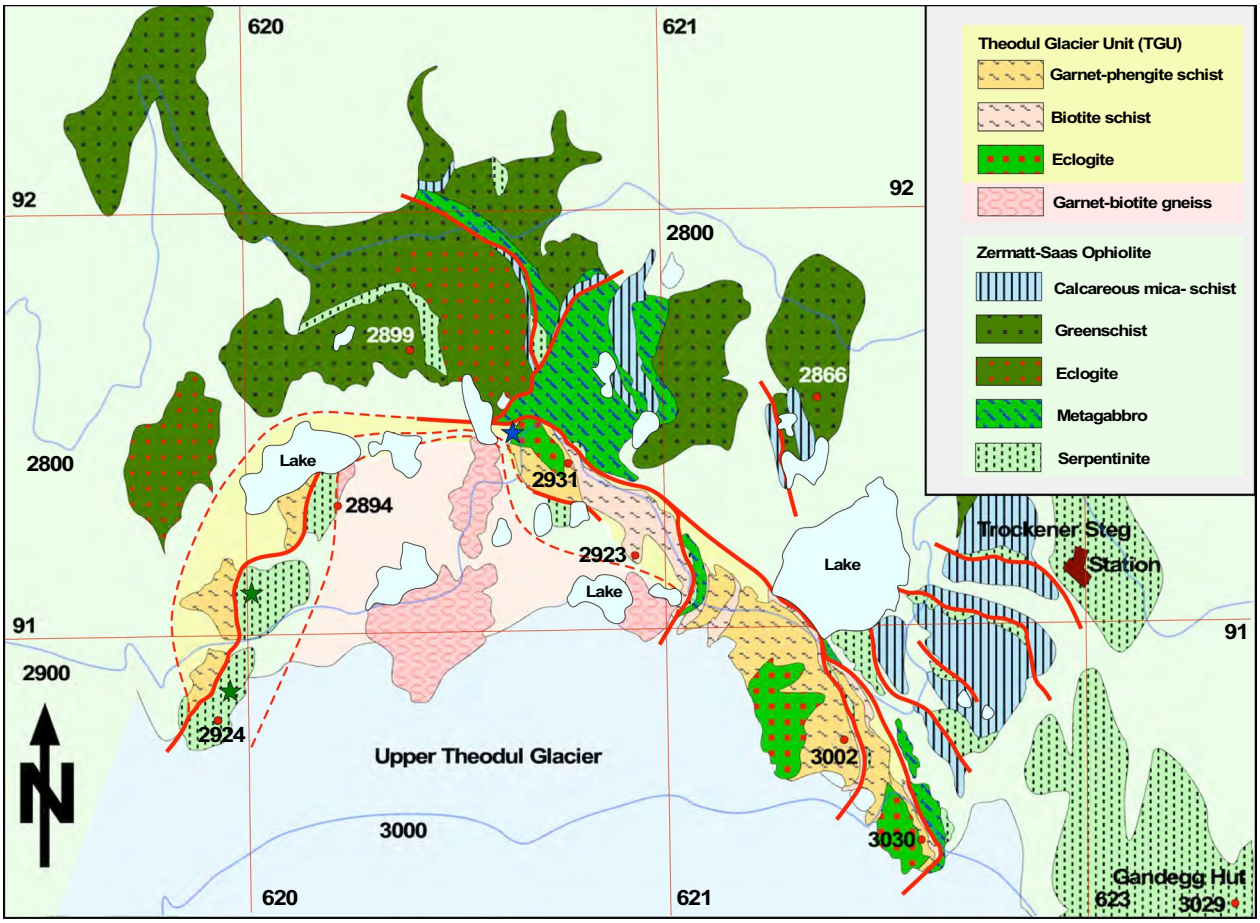

Fig. 3 Geological map of the Trockener Steg area with the sampling location of eclogite of SW9 (blue star) and two rodingite occurrences (green stars). The key samples of the Grt-Ph schists KB860 and OK-Z133 (Bucher et al. 2019) have been collected at the SE-wall of point 3030 (see also Fig. 4) (OK samples from Klemm 2005). Note that the map is a revised and improved version of the local geological map in Weber and Bucher (2015). Easting and northings according to the Swiss coordinate network

Zermatt-Saas ophiolites about 100 m below the basal thrust of the Combin Unit (Fig. 2). The TGU slab is imbricated and has been transected by secondary thrusts and ZSU material, predominantly serpentinites but possibly also eclogite (Figs. 3 and 4). The basal main thrust fault separating the TGU from ZSU cuts minor thrusts in the ZSU. The slab is covered by ZSU serpentinites along a top thrust (Fig. 3). The serpentinite outcrops near point 2924 (green stars on Fig. 3) expose two types of meta-rodingites (Li et al. 2004b, 2008). A separate slice of garnet-biotite gneiss rests on the TGU and ZSU rocks (Fig. 3).

3.2 Rock assemblage

The three rock types of the TGU are tectonically interleaved and the variability at outcrop scale is much larger than shown on the simplified geological map (Fig. 3). Garnet-phengite schist represents the most abundant rock type of the TGU (Fig. 4). The cm-large garnet porphyroblasts show a complex internal chemical structure. The core regions of the garnets formed under granulite facies conditions whilst a younger generation of garnet material in the schists can be related to eclogite facies metamorphism (Bucher et al. 2019). Lenses, boudins and blocks of eclogite from some centimeters to many meters in size are common within the Grt-Ph schists (Fig. 5a) (all abbreviations for mineral names after Whitney and Evans 2010). Banded eclogite in Grt-Ph schist can be broken and rotated (Fig. 5b). The composition of the TGU eclogites is distinctly different from the ZSU eclogites and suggests a within-plate origin of the original mafic rocks rather than being ophiolitic (Weber and Bucher 2015). The eclogites contain abundant Qz and Ph in addition to Grt and Omp in contrast to Qz-absent ZSU eclogites with abundant Pg, Mg-Cld and Gln. The TGU eclogites contain as well a notable amount of Zrn contrary

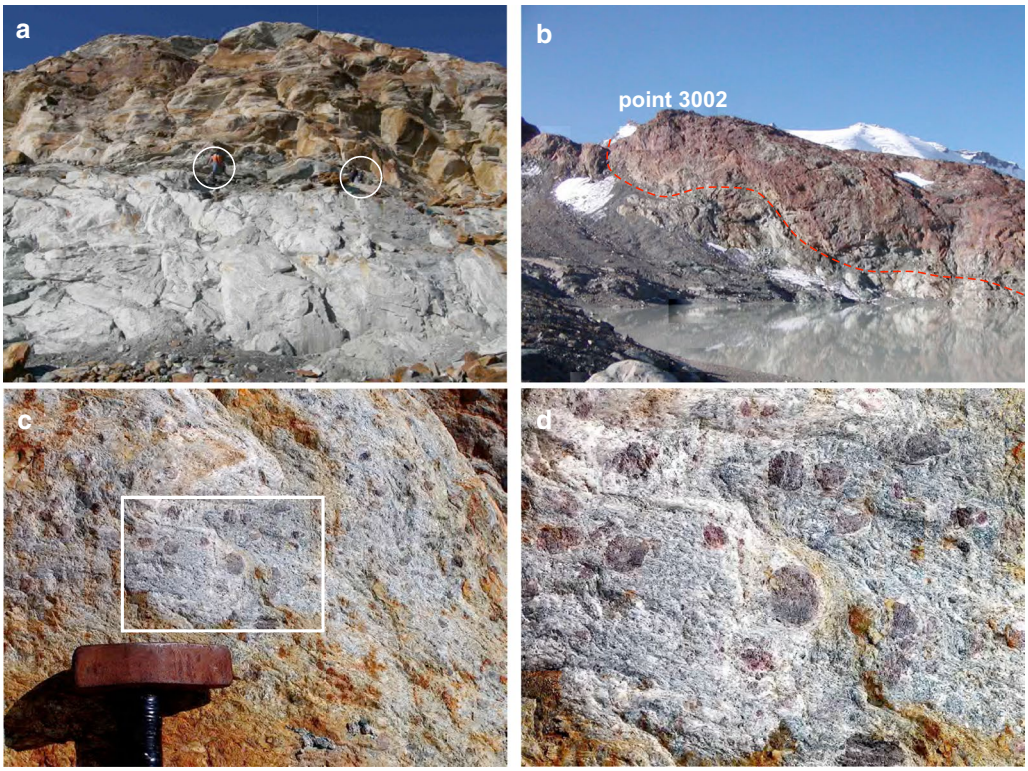

Fig. 4 **a** NE-face of point 3030. Low ground: Light-gray foliated meta-gabbro of the ZSU with well-preserved omphacite. Top part of wall: Rusty-weathering Grt-Ph schists (sampling site of KB860 and OK-Z133) and Bt-gneiss (Fig. 3). The basal thrust of the Theodul Glacier Unit in the middle of the wall and is well marked with small serpentinite lenses (e.g. at the position of the two geologists in white circles). **b** Point 3002 seen from north (Figs. 2 and 3). Basal thrust of TGU marked with red dashed line (ZSU above the lake, TGU at the top). Along the thrust several small serpentinite lenses occur. Rusty TGU rocks are predominantly Grt-mica-schists. Eclogites and Bt-gneiss are greyish colored. **c** Garnet-phengite schist at outcrop scale. Note cm sized and euhedral undeformed garnet (hammer head is 12 cm). **d** Close-up of framed area on **c**

to the ZSU eclogites. The eclogite facies metamorphism occurred about 57 Ma ago, in the late Paleocene, as indicated by Lu–Hf garnet-whole rock analyses of TGU eclogites (Weber et al. 2015). The Bt gneiss and Bt schist shown on the geological map (Fig. 3) are not described in this paper.

4 Methods

The composition of minerals was determined using a CAMECA SX-100 electron microprobe at the University of Freiburg. All quantitative analyses were made using wavelength-dispersive spectrometers. Operating conditions were 15 kV acceleration voltage and 15 to 20 nA beam current with counting times of 10 s and a focused electron beam. Mica was measured with a defocussed beam (5 µm) to minimize the effect of Na and K loss during analysis. The instrument was calibrated for each element analyzed using well-characterized natural materials as standards. Data reduction was performed utilizing PAP software provided by CAMECA.

Whole rock analysis was performed by standard X-ray fluorescence (XRF) techniques at the University of Freiburg, Germany, using a Philips PW 2404 spectrometer. Pressed powder and Li-borate fused glass discs were prepared to measure contents of trace and major elements, respectively. Raw data were processed with the standard XR-55 software of Philips. Relative standard deviations 2σ are < 1 and $< 4\%$ for major and trace elements, respectively. Loss on ignition was determined by heating at 1100 °C for 2 h. Rare earth elements (REE) analyses were performed by sodium peroxide fusion ICP AES at SGS Minerals Services in Lakefield, Ontario Canada.

P–T conditions during the different stages of metamorphism have been deduced from thermodynamic models using Theriak/Domino software of de Capitani and Petrakakis (2010), and thermodynamic data from Berman (1988) (JUN92 data and updates). The thermodynamics of Grt, Cpx and white mica solutions follow the models of Berman (1988), Meyre et al. (1997) and Keller et al. (2005), respectively.

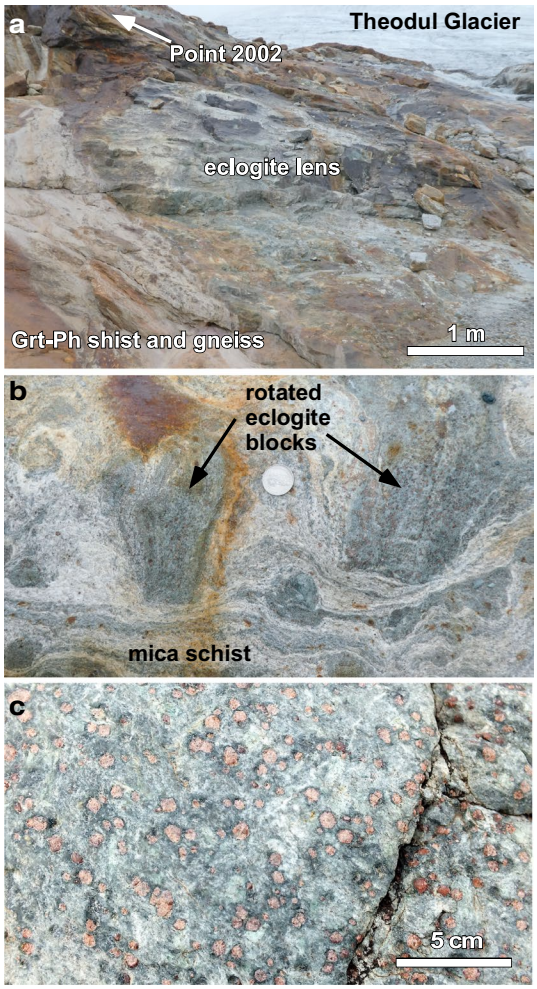

Fig. 5 Outcrops of TGU eclogites at the W-slope of point 3002 (Fig. 2). **a** eclogite lens within Grt-Ph schist. **b** Rotated blocks of banded and foliated eclogite in Grt-Ph schist matrix. **c** eclogite with ~ 10% modal euhedral garnet of 2–5 mm in diameter in a matrix of relic Omp, Cam, Ph, Pg, Chl, Ep, Qz, and accessories

Dating was carried out with U–Pb isotope dilution thermal ionization mass spectrometry (ID-TIMS). Zircon grains were selected under a binocular microscope and subjected to chemical abrasion (Mattinson 2005) before spiking with a ^{202}Pb–^{205}Pb–^{235}U tracer, dissolution, and mass spectrometry, following the procedure of Krogh (1973) with modifications described in Corfu (2004). The data were corrected for blanks of 0.1 pg U and ≤ 2 pg. The remaining initial Pb was corrected using compositions calculated with the model of Stacey and Kramers (1975). Plotting and regressions were done with the Isoplot software package (Ludwig 2009). The decay constants are those of Jaffey et al. (1971). Uncertainties in the isotope ratios and the ages are given and plotted at 2σ.

5 The eclogites

Samples of TGU eclogite have been collected and studied across the TGU (Fig. 3) during fieldwork from 2005 to 2015 (Weber and Bucher 2015). Sample SW9 used for Zrn dating comes from the locality marked with a blue star on the geological map (Fig. 3). The exact location has the coordinates: 620,650 easting, 91,470 northing (Swiss coordinate network).

Sample SW9 contains the minerals Grt, Cam, Pl, Chl, Ph, Pg, Rt, Ttn, Qz, and Zrn. The early Alpine high-pressure assemblage Grt + Omp has been replaced by the later assemblages with Pl, Cam, Chl and Ttn. The rock contains also subordinate amounts of Qz, Pg and Zrn. Small grains of Ap, Ep and sulfide (mostly Py) are also present. There are no Omp relics preserved in this sample, in contrast to many other partially retrogressed basic meta-volcanic rocks from the TGU (Weber and Bucher 2015). The texture of the SW9 rock is dominated by coarse well-aligned optically zoned Cam. Pl forms an equilibrated texture with Cam. Grt is euhedral and strongly poikilitic. The Grt are typically rimmed with a thin seam of late Chl (see also Fig. 5c). The mineral inclusions comprise Rt, Qz, and Pg and show sigmoidal trails indicative of rotation during growth. Grt has no Cam inclusions.

Bulk K_2O is relatively low in SW9, which is reflected by low modal Ph. It occurs together with abundant Pg as a fine-grained mineral in the Cam-rich matrix. Abundant Chl occurs in association with Ph and Pg and occasionally as a late replacement of Grt. In the foliated Cam-mica matrix of the rock, Chl locally grows across the foliation.

5.1 Composition of the SW9 eclogite and its minerals

The chemical composition of the mafic metavolcanic sample SW9 is given for major and some trace elements on Table 1. The composition of SW9 is similar to those of other mafic rocks including all eclogites of the TGU. The TGU metavolcanic rocks derive from typical "within plate basalts" in contrast to mafic rocks of the ZSU, which are "MOR or OI basalts" (Weber and Bucher 2015).

Garnet is compositionally zoned with Grs-rich Prp-poor cores and a mantle (rim) richer in Prp and lower in Grs (Table 2). There is more Sps in the core than Prp. Sps decreases rapidly towards the mantle where it is very low. This features are typical of prograde zonation in Grt. The core area is about 40% of the Grt diameter. Consequently, the core stands for 6 vol.% of the total Grt volume, the

Table 1 Composition of TGU eclogite SW9

Major el.	wt%	Trace el.	ppm
SiO_2	46.25	Ba	18
TiO_2	3.00	Co	52
Al_2O_3	13.03	Cr	589
FeO[a]	11.87	Cu	34
MnO	0.19	Nb	50
MgO	9.10	Ni	203
CaO	11.75	Pb	5
Na_2O	1.91	Sc	29
K_2O	0.09	Sr	337
P_2O_5	0.46	V	283
LOI	1.57	Y	30
Total	99.22	Zn	164
		Zr	231
#Mg[b]	0.58	Rb	0

[a] Total iron as FeO

[b] #Mg = Mg number (Mg/(Mg + Fe)) in atoms, LOI = loss on ignition

Table 2 Composition of eclogite facies garnet in SW9

	Core			Rim
SiO_2	37.41	37.43	37.43	37.17
TiO_2	0.12	0.1	0.1	0.1
Al_2O_3	21.17	21.28	21.28	20.99
FeO	25.37	27.92	27.92	28
MnO	2.67	0.54	0.54	0.11
MgO	1.04	1.56	1.56	1.94
CaO	12.05	11.14	11.14	10.72
Total	99.83	99.97	99.97	99.03
Si	2.985	2.979	2.977	2.980
Ti	0.007	0.006	0.006	0.006
Al	1.991	1.996	1.995	1.983
Fe^{2+}	1.693	1.857	1.857	1.877
Mn	0.180	0.036	0.042	0.009
Mg	0.124	0.184	0.185	0.232
Ca	1.030	0.949	0.949	0.921
Sum	8.010	8.007	8.012	8.008
Pyrope	4.09	6.11	6.10	7.63
Almandine	55.92	61.34	61.21	61.78
Spessartine	5.96	1.2	1.40	0.29
Grossular	34.03	31.35	31.29	30.30

Total includes traces of Na.K and Cr

mantle and rim represent 94 vol.% of the Grt. There is about 10 vol.% modal Grt in SW9 (Fig. 5c). Grt core material represents 0.6 vol.% of modal Grt. Therefore, it is not necessary to correct the bulk rock composition for the fractionation into the Grt core for the *P–T* model for the Grt mantle and rim growth presented below.

The Si content of phengite reaches 3.35 atoms per formula unit (a.p.f.u.). Phengite contains about 10 mol% Pg component and X_{Mg} is 0.72 in Cel-rich Ph and 0.63 in late Ms-rich Ph (Table 3). Chlorite occurs in different generations and compositions, the first being Mg-rich, the last Fe-rich (Table 3). All amphiboles are Ca-amphiboles but differ considerably in composition (Table 4) and can be classified as actinolite and magnesio-hornblende (Hawthorne et al. 2012). The Al-content varies from 0.5 in Act and increases to 1.5 a.p.f.u. in Mhb. Between 0.7 and 2 wt% Na indicates that Cam developed from Omp originally present. Plagioclase is an oligoclase with An ~ 21 (Table 5).

5.2 P–T model for eclogite SW9

P–T estimates have been obtained utilizing the Theriak/Domino software (de Capitani and Petrakakis 2010) using rock and mineral composition data presented above (Fig. 6). The rock composition (Table 1) has been simplified to the model system as follows: TiO_2 is predominantly present in rutile. A small amount of TiO_2 is present in titanite formed during retrogression and has been ignored. 0.2 wt% MnO has been ignored. The rock contains 0.46 wt% P_2O_5 present in Ap ($Ca_5(PO_4)_3(OH)$). Thus a stoichiometric amount of 0.43 wt% Ca has been subtracted from the rock composition given in Table 1. The remaining components are included in the phase equilibrium model.

The first Grt appears at about 500 °C and 1.5 GPa in rocks with the composition of SW9 (Fig. 6a) along a subduction geotherm of 9.5 °C/km. The computed first Grt has the composition Grs 35, Prp 8, Alm 57 (Fig. 6b). The core of the measured SW9 Grt has Grs 34 but a much lower Prp of 4. This mismatch is related to the presence of 6 mol% Sps in the core, which is not adequately modeled here (Konrad-Schmolke et al. 2008). The onset of Grt growth strongly fractionates MnO into the core of the new Grt thus expanding its stability field to lower temperature. This results in a lower temperature for the first Grt with a lower Prp of the core.

The mantle and rim of Grt representing > 90 vol.% of the Grt contains 30 mol% Grs component, 8 mol% Prp, 62 mol% Alm and only traces of Sps (Table 2). For this Grt composition the three isopleths intersect at 503 °C and a slightly higher pressure of 1.63 GPa (point 1 Fig. 6b). However, the Grt isopleths intersect at a second point (point 2 Fig. 6b) at 510 °C and 1.3 GPa. Yet the Grs isopleth are narrow spaced and vertical at point 2, which would lead to strongly Grs zoned Grt during prograde metamorphism. The SW9 garnet shows a very small Grs variation from 34 in the very core to 30.4 mol% in the outer rim zone (Table 2) in agreement with the orientation and spacing of the Grs isopleths

Table 3 Composition of phengite, paragonite and chlorite in TGU eclogite SW9

	Ph	Ph	Pg	Pg	Chl 3	Chl 2	Chl 1
SiO_2	52.41	48.59	48.28	48.77	26.56	25.52	24.31
TiO_2	0.08	0.15	0.04	0.06	0.06	0.12	0.06
Al_2O_3	29.87	32.78	40.23	41.44	20.9	19.24	20.4
FeO	2.43	2.18	0.37	0.31	21.6	29.57	31.81
MnO	0.05	0.03	0.01	0.03	0.06	0.34	0.54
MgO	3.46	2.07	0.28	0.12	17.4	12.33	10.29
CaO	0.02	0.12	0.13	0.16			
Na_2O	0.67	0.5	6.67	6.59			
K_2O	9.8	9.34	1.11	0.46			
Total	98.81	96.1	97.28	98.17	87.01	87.39	88.05
Si	3.353	3.231	3.019	3.007	2.764	2.774	2.663
Ti	0.004	0.008	0.002	0.003	0.005	0.01	0.005
Al	2.253	2.569	2.965	3.012	2.564	2.465	2.634
Fe^{2+}	0.130	0.121	0.019	0.016	1.880	2.688	2.914
Mn	0.003	0.002	0.000	0.002	0.005	0.031	0.050
Mg	0.330	0.205	0.026	0.011	2.699	1.998	1.680
Ca	0.002	0.009	0.009	0.011			
Na	0.083	0.064	0.808	0.788			
K	0.800	0.792	0.089	0.036			
X_{Mg}	0.72	0.63	0.57	0.41	0.589	0.426	0.365

Mica: Total includes traces of Cr. Traces of F and Cl are close to or below detection limit. XMg = Mg/(Mg + Fe)

Chlorite: Totals contain traces of Cr, Ca, Na and K. (1) chlorite in direct contact to garnet; (2) matrix chlorite intergrown with paragonite; (3) chlorite veins in garnet

at point 1 (Fig. 6b). Modeled Si in Ph is close to 3.38; measured Ph has a Si of 3.35 (Table 3). The predicted stable assemblage at these *P–T* conditions is: Grt-Omp-Ph-Pg-Chl-Qz-Lws. The assemblage is present in SW9 except for Omp and Lws, which have been replaced mostly by Cam during greenschist facies recrystallization. At point 1 Gln is not part of the stable assemblage but it is present at lower temperature before the first Grt forms. Plagioclase (oligoclase) in the rock matrix is not predicted to be stable under these *P–T* conditions. The computed modal Grt of 7 vol.% matches modal Grt of ~ 10 vol.% in the sample SW9 reasonably close. The observed composition of the Grt suggests that the rock has not been subducted to conditions beyond point 1 (Fig. 6a) corresponding to 53 km depth (rock density 3000 kg/m^3). With increasing *P–T* Grs decreases and Prp increases significantly and reach 24% Grs and 23% Prp at 600 °C and 2 GPa, for example. At these conditions predicted modal Grt would be > 40 vol.% in contrast to the observed ~ 10 vol.%.

The matrix assemblage Pl An_{20} + Mhb can be related to a later post-eclogite recrystallization. The modeled *P–T* conditions during this matrix recrystallization are ~ 450 °C and 550 MPa (Theriak model). Computed Pl has An_{25} and Ca-Amp contains 81 mol% Prg in agreement with analyzed Pl and Amp (Tables 4 and 5). Computed X_{Mg} in Chl of 0.5 compares with the measured X_{Mg} = 0.4 for Chl in the matrix of SW9 (Table 3).

5.3 Characteristics of SW9 zircons

The population is composed largely of equant to short-prismatic grains, generally highly subrounded. Cathodoluminescence images reveal complex textures, in part with straight, regular zoning (Fig. 7a) or with more random mosaic-type textures (Fig. 7b). The grain in Fig. 7c is characterized by a CL-dark internal domain surrounded by a CL-bright outer zone showing a very faint regular growth zoning. All zircons show variable evidence of reworking resulting in dissolution, recrystallization and the formation of veins, locally thin CL bright overgrowths and zones of disrupted and convolute zoning. This feature is most strongly developed in grain of Fig. 7d, both in the CL-dark core and in the CL-bright rim.

5.4 U–Pb results

The data include one fraction of 8 small round grains (too small for single-grain analysis), and 7 single grain analyses (Table 6). The data show a high degree of

Table 4 Composition of amphiboles in eclogite facies SW9

	Act	Act	Hbl	Hbl	Hbl
SiO_2	55.2	53.96	45.96	48.78	49.08
TiO_2	0.01	0.05	0.2	0.22	0.13
Al_2O_3	3.23	5.79	6.65	7.77	9.21
FeO	7.88	6.74	20.51	16.2	12.97
MnO	0.05	0.03	0.39	0.47	0.04
MgO	18.01	17.78	10.59	11.59	12.88
CaO	11.02	9.67	9.94	10.16	9.95
Na_2O	1.26	2.12	0.71	1.30	1.98
K_2O	0.07	0.19	0.07	0.12	0.11
Cl	0	0	0.02	0.01	0.01
F	0.23	0.26	0.14	0.15	0.24
Total	96.98	96.67	95.24	96.92	96.71
Si	7.805	7.617	7.112	7.235	7.173
Ti	0.000	0.005	0.023	0.025	0.014
Al	0.538	0.963	1.213	1.358	1.586
Fe^{2+}	0.932	0.796	2.654	2.009	1.585
Mn	0.006	0.004	0.051	0.059	0.005
Mg	3.796	3.742	2.443	2.563	2.806
Ca	1.670	1.463	1.648	1.615	1.558
Na	0.345	0.580	0.213	0.374	0.561
K	0.013	0.034	0.014	0.023	0.021
Sum cations	15.105	15.203	15.372	15.260	15.310
Al(IV)	0.195	0.383	0.888	0.765	0.827
Al(VI)	0.343	0.580	0.325	0.593	0.760
Sum Al(VI), Ti, Fe, Mn, Mg	5.272	5.509	6.385	6.014	5.997
X_{Mg}	0.803	0.825	0.479	0.560	0.639
Sum Ca, Na, K	2.028	2.077	1.875	2.011	2.140

Total includes traces of Cr. $X_{Mg} = Mg/(Mg + Fe)$

Table 5 Composition of plagioclase in SW9

	1	2
SiO_2	62.60	62.57
Al_2O_3	23.29	23.55
FeO	0.09	0.06
MgO	0.00	0.00
CaO	4.33	4.46
Na_2O	9.24	8.91
K_2O	0.10	0.09
Total	99.79	99.71
Si	2.780	2.776
Al	1.219	1.231
Fe^{2+}	0.003	0.002
Mg	0.000	0.000
Ca	0.206	0.212
Na	0.795	0.766
K	0.006	0.005
SUM	5.011	4.994
Ab	78.98	77.92
An	20.46	21.56
Or	0.56	0.52

Total includes traces of Ti, Cr and Mn

dispersion with U–Pb ages ranging from about 290 to 150 Ma (Fig. 8). Six of the analyses define a line (with an MSWD of 3.1) having intercept ages at 295 ± 16 Ma and 145 ± 34 Ma. The oldest analysis deviates to the right of the line, suggesting the presence of an older component probably related to the magmatic stage. However, the extrusion age of the basalts could not be quantified and remains unknown. The granulite facies event at 295 Ma whiped out the magmatic age. The two youngest analyses also deviate from the line. They represent grains that became highly turbid after chemical abrasion, the youngest one an isolated tip. They were analyzed to test the lower intercept age of 145 Ma, whether it could be confirmed and whether it might correspond to an event that formed new zircon. The results do not provide a conclusive answer to this question, but they show that at least some of the discordance is due to younger overprints, likely during the Alpine events.

Considering the combination of observed textures and the complex, but broadly coherent data, it can be concluded that the upper intercept age of 295 ± 16 Ma corresponds to the time of high-grade metamorphism, consistent with the mosaic textures seen in part of the zircon grains (Fig. 7b). The analysis with the slightly older age may reflect an original magmatic zircon component, possibly represented by regular zoned grains such as seen in Fig. 7a. The reasons for the subsequent strong disturbance of the U–Pb systems are less clear, but it was likely related to the extensive reworking of zircon documented in textural features such as seen in Fig. 7b, c. The lower intercept age of 145 ± 34 Ma suggests that the event could have been associated with hyperextension processes during continental breakup and the initiation of the Tethys in the Mid-Jurassic (Dogger). The zircon U–Pb systems were in part also affected during the Alpine events that formed, and then retrogressed, the eclogite.

6 The garnet-phengite schists

Garnet data from the TGU garnet-phengite schist (Figs. 4c, d) have been presented by Bucher et al. (2019). Two porphyroblastic Grt samples, KB860 and OK-Z133, exhibit particularly well-developed internal chemical structures in garnet and have been studied in detail. Here, we supplement additional data from TGU Grt-Ph schists and refine the *P*–*T* history deduced by Bucher et al. (2019). There are new *P*–*T* data for the Grt-Ph schists for the post-eclogite stages and matrix-recrystallization.

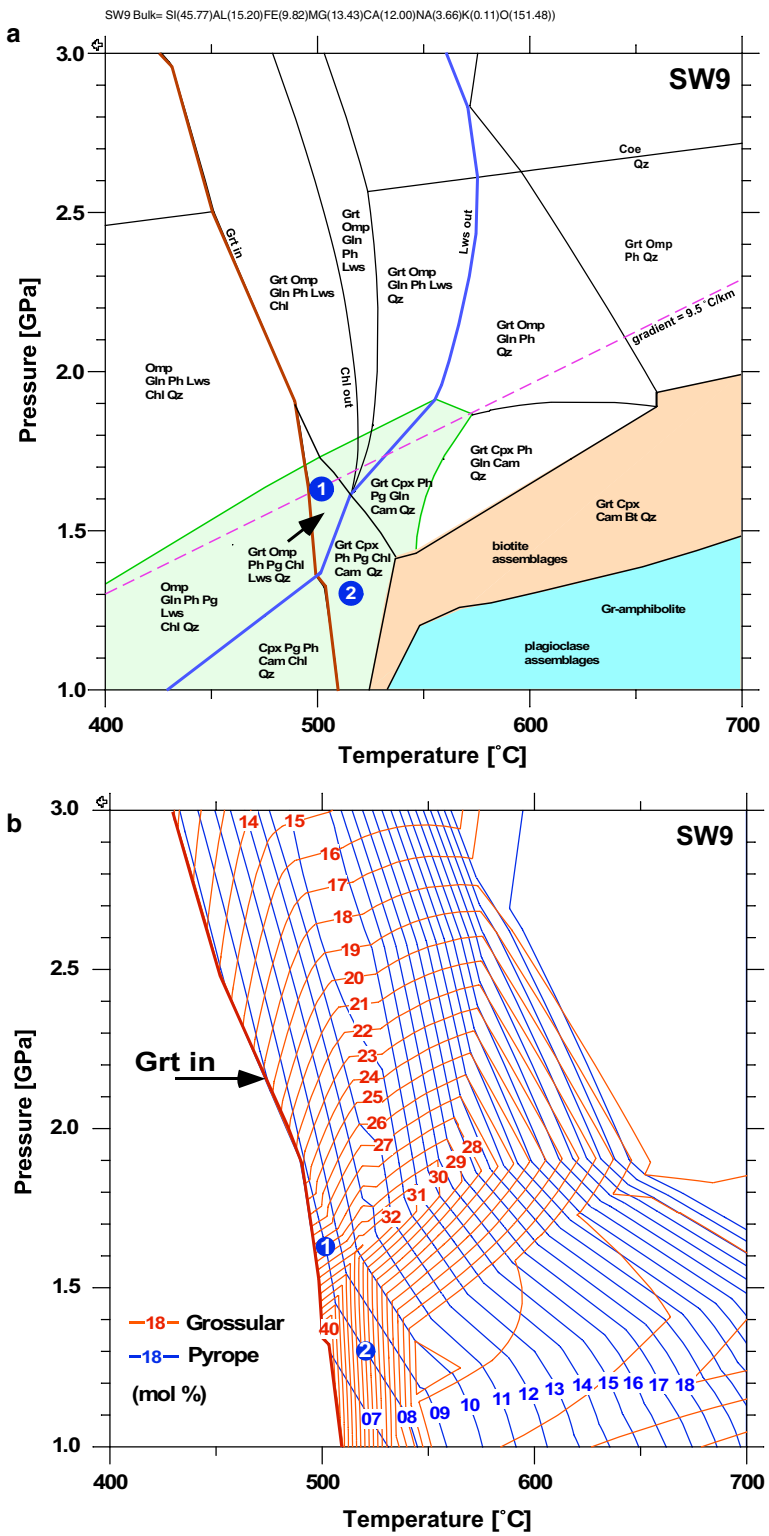

Fig. 6 *P–T* diagrams for the sample SW9. The SW9 bulk is apatite corrected and ignores TiO_2 and MnO (see text). Models from Domino software (de Capitani and Petrakakis 2010). **a** Green field for Pg present assemblages. Blue points 1 and 2 are at *P–T* conditions for the Grt $Grs_{30}Prp_8$ from **b**. Dashed violett line marks a linear gradient of 9.5 °C/km. **b** Grt composition isopleths for Grs and Prp with two intersections (blue points) for the measured Grt mantle and rim $Grs_{30}Prp_8$ in the sample SW9

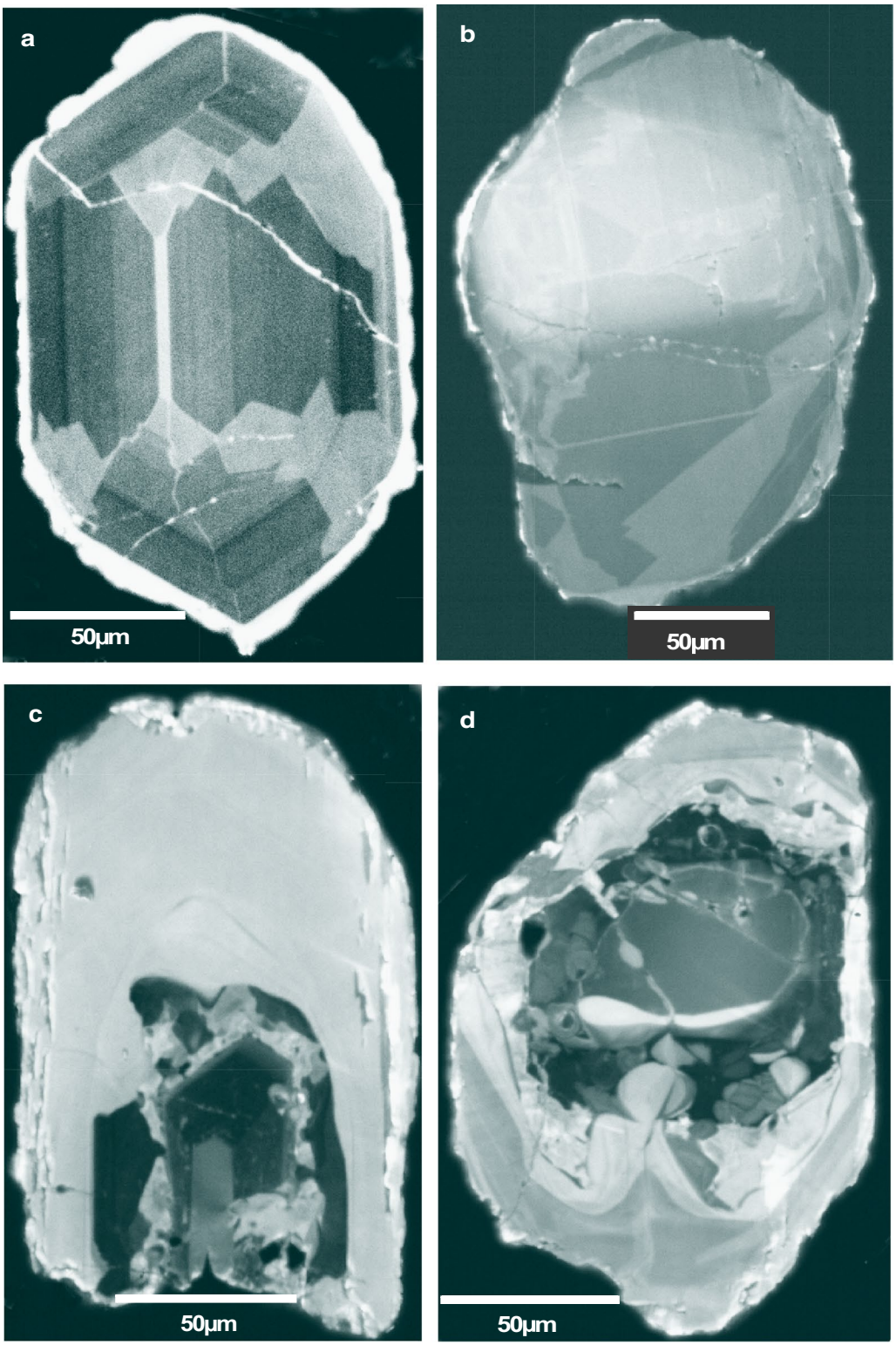

Fig. 7 Cathodoluminescence (CL) images of zircon from eclogite SW9. **a** Short prism with straight regular zoning, surrounded by a thin rim of CL-bright zircon, the same material also coating fractures at the interior of the grain. **b** Mosaic textured zircon. **c** A CL-dark internal domain with regular zoning but also recrystallized CL-bright domains is surrounded by a CL-bright outer zone showing a very faint regular growth zoning. **d** Complex chaotic texture with a CL-dark internal domain surrounded by CL-bright rim and cut by similar veins, all parts of the grains suggesting extensive metamorphic recrystallization

Table 6 Zircon U–Pb data

Properties	Weight µg	U ppm	Th/U	Pbc pg	206/204	207/235 abs	2 σ	206/238	2 σ abs	rho	207/206	2σ abs	206/238 Ma	2 σ abs	207/235 Ma	2 σ abs	207/206	2 σ abs	Disc %
(a)	(b)	(b)	(c)	(d)	(e)	(f)	(f)	(f)	(f)	(f)	(f)	(f)	(f)	(f)	(f)	(f)	(f)	(f)	
Z sp [1]	1	406	0.41	0.7	1607	0.32095	0.00197	0.044239	0.000134	0.63	0.05262	0.00025	279.1	0.8	282.6	1.5	312.4	11.0	10.9
Z eq sbr [1]	8	266	0.49	1.2	4729	0.30898	0.00094	0.043071	0.000090	0.78	0.05203	0.00010	271.8	0.6	273.4	0.7	286.7	4.3	5.3
Z eq sbr-an [1]	2	1108	0.45	0.7	7803	0.30006	0.00128	0.041944	0.000160	0.93	0.05188	0.00008	264.9	1.0	266.4	1.0	280.3	3.6	5.6
Z eq sp [1]	5	169	0.48	2.4	922	0.29227	0.00212	0.040928	0.000083	0.47	0.05179	0.00034	258.6	0.5	260.3	1.7	276.2	14.9	6.5
Z eq sbr [8]	1	1494	0.43	0.9	4101	0.28710	0.00131	0.040394	0.000142	0.86	0.05155	0.00012	255.3	0.9	256.3	1.0	265.4	5.4	3.9
Z eq an [1]	9	210	0.44	1.1	4385	0.28123	0.00091	0.039515	0.000084	0.75	0.05162	0.00011	249.8	0.5	251.6	0.7	268.5	4.9	7.1
Zslp-fr cloudy [1]	10	379	0.60	2.6	2980	0.22602	0.00078	0.032233	0.000073	0.76	0.05086	0.00012	204.5	0.5	206.9	0.6	234.3	5.2	12.9
Z eu sp cloudy [1]	13	235	0.57	1.0	5213	0.19878	0.00055	0.028413	0.000055	0.80	0.05074	0.00009	180.6	0.3	184.1	0.5	229.1	3.9	21.5
Z tip cloudy [1]	1	503	0.47	5.5	159	0.17242	0.00436	0.024368	0.000090	0.39	0.0513	0.0012	155.2	0.6	161.5	3.8	255.1	54.5	39.6

(a) All zircon grains treated with chemical abrasion (Mattinson 2005); eq = equamt; sp = short-prismatic; sbr = subrounded; an = anhedral: fr = fragment [1] = number of grains

(b) Weight and concentrations are known to better than 10%, except those of about 1 µg know to about 50%

(c) Th/U model ratio inferred from 208/206 ratio and age of sample

(d) Pbc = total common Pb in sample (initial + blank)

(e) Raw data, corrected for fractionation and spike

(f) Corrected for fractionation, spike, blank (206/204 = 18.3; 207/204 = 15.555) and initial common Pb (based on Stacey and Kramers 1975); error calculated by propagating the main sources of uncertainty

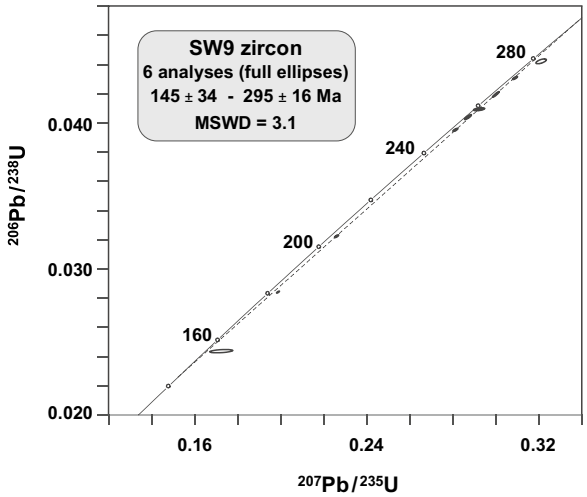

Fig. 8 Concordia diagram. Ellipses around individual data points indicate 2σ uncertainty. Upper intercept age of 295 ± 16 Ma is interpreted to reflect granulite facies metamorphism. The significance of the lower intercept is more uncertain; it is possible that isotopic resetting could have been caused by the processes related to Jurassic hyperextension, with further disturbances during the Alpine events

Furthermore, there are previously unpublished rock and mineral composition data presented and discussed in this section (e.g. REE and traces of the rock). Since the study by Bucher et al. (2019) focussed on Grt, there are few other mineral analyses given in that paper. Here, the composition of matrix minerals are presented in Tables 9, 10, 11, 12 and used for an improved derivation of the post-eclogite metamorphism.

The Grt-Ph schists contain euhedral Grt porphyroblasts (Fig. 4c, d) occurring in a matrix of Ph, Pl, Chl, Pg, and modally subordinate Ep, Qz, Ttn, Rt, rare Amp, and Fe-sulphide (Fig. 9a). The Ph- and Chl-rich rocks are well foliated (Ph, Pg, Chl > 70% modal). The texture of some samples bears evidence for two generations of Ph (Fig. 9b).

Large porphyroblastic Grt crystals consist of an aggregate of angular and blocky fragments of first generation Grt with a second generation of Grt material between the fragments and along the rims of the porphyroblasts. The first generation of Grt is rich in Prp component and formed by pre-Alpine granulite facies metamorphism. The late generation of garnet is low in Prp and rich in Grs component. It was formed during Alpine eclogite facies metamorphism (Bucher et al. 2019).

The dominant mica is a fine-grained Ph forming the schistose structure. It occurs intergrown with Pg and also occurs as fine inclusions within Pg. Abundant Chl is present in association with Ph and Pg and locally grows across the foliation. Epidote appears as small (< 50 µm)

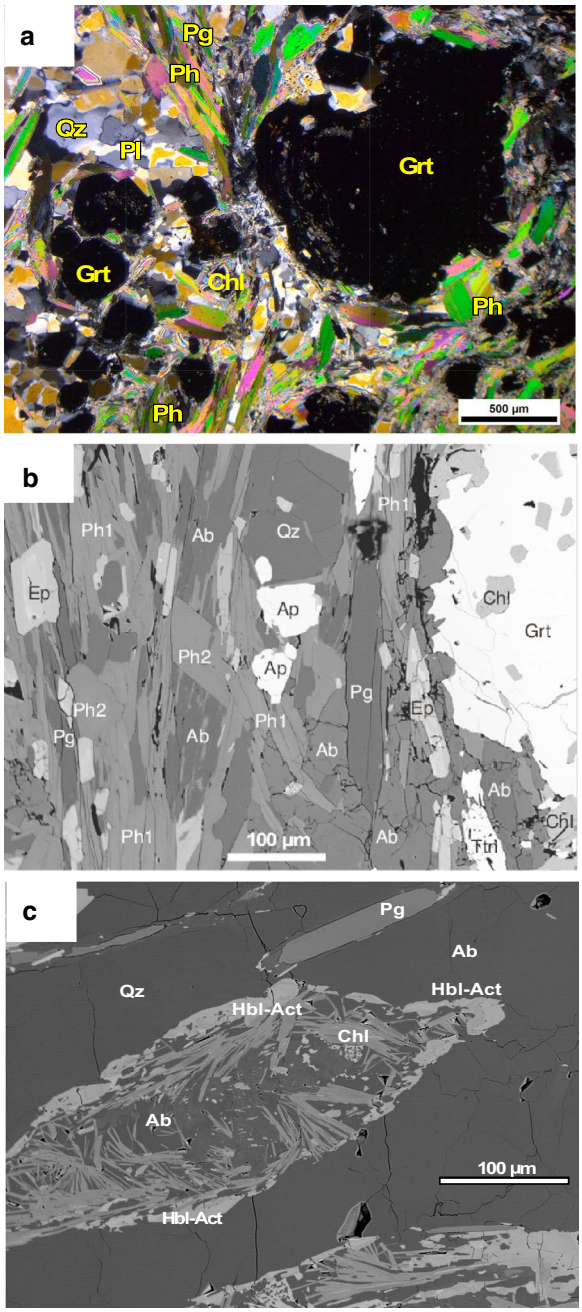

Fig. 9 **a** Photomicrograph of texture and mineral assemblage of sample KB860 (cross-polarized light): Grt, Qz, Pl, white mica and Chl. **b** Backscattered electrons (BSE) image of texture and mineral assemblage of sample OK-Z131. A predominant generation of foliation-parallel Ph (Ph1) with Si = 3.3 has been overgrown by a later generation of Ph with Si = 3.1 (Ph2). **c** Backscattered electrons (BSE) images showing a Chl–Ab pseudomorph after Gln in sample OK = Z129. Scale bar = 100 µm. The pseudomorph is rimmed by Mhb and Act

euhedral grains with trapezoidal cross section locally overgrowing corroded REE Ep, allanite (Fig. 9b). Plagioclase is a member of the matrix assemblage together with the white micas and Chl. Amphibole occurs locally as a minor phase associated with Pl. The presence of Chl-Ab pseudomorphs after Amp rimmed by Act suggest that Gln was present in the rock at some earlier stage (Fig. 9c). Accessory Ttn locally replaces Rt.

6.1 Rock and mineral composition

6.1.1 Rock

The major element composition of the Grt-Ph schist sample KB860 is given in Bucher et al. (2019). KB860 is a terrigenous clastic rock and classifies as shale. The relatively high CaO suggests that the shale contained carbonate (calcite) prior to the first metamorphism and that the sedimentary protolith classifies as calcareous mudstone. Here we present new REE and other trace element concentration data analyzed in addition for a complete characterization of the modeled material (Table 7). The total rare earth element (REE) content of 293 ppm is enriched relative to chondrite values (Fig. 10a). The chondrite-normalized REE pattern decreases regularly from La to Sm but it becomes more flat at the heavy rare earth elements

Table 7 Composition of KB860, trace elements (ppm)

Li	–	Cs	1.8
Be	–	Ba	852
B	–	La	61.2
Sc	25	Ce	122
V	160	Pr	14.4
Cr	163	Nd	53.3
Co	27.4	Sm	9.4
Ni	86	Eu	1.96
Cu	22	Gd	8.8
Zn	140	Tb	1.35
Ga	30	Dy	8.46
Ge	2	Ho	1.68
As	–	Er	4.67
Rb	113	Tm	0.67
Sr	144	Yb	4.2
Y	45.4	Hf	5
Zr	197	Ta	1.3
Nb	26	W	2
Lu	0.65	Tl	0.5
Mo	–	Pb	b.d.l.
Ag	–	Bi	b.d.l.
In	–	Th	21.3
Sn	–	U	2.18
Sb	–		

– Below detection limit

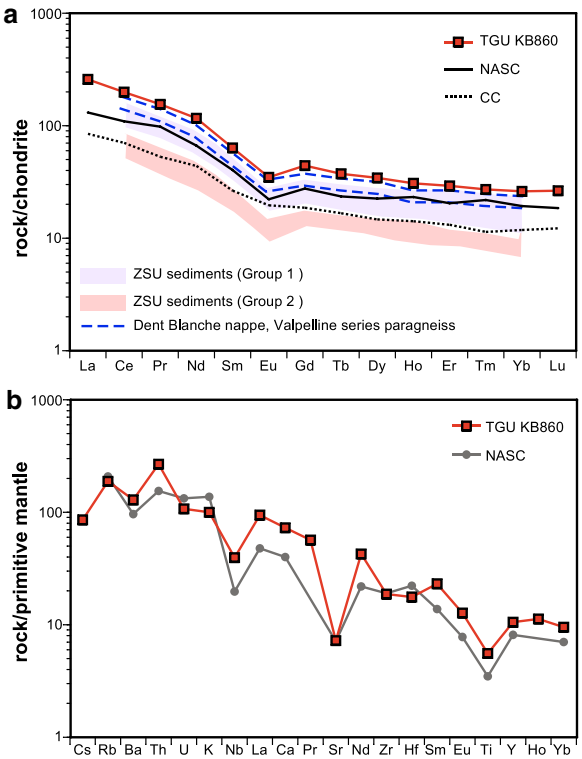

Fig. 10 Trace element composition of garnet-phengite schist KB860. **a** Chondrite-normalized REE patterns. Chondrite data for normalization from McDonough and Sun (1995). For comparison NASC (North American shale composite) from Gromet et al. (1984); CC (continental crust) from Rudnick and Gao (2003), ZSU metasediments (Group 1 and 2 from Mahlen et al. 2005), paragneiss from the Valpelline series of the Dent Blanche nappe (Mahlen et al. 2005). b) Multiple trace element diagram (spider diagram). Primitive mantle data for normalization from McDonough and Sun (1995). For comparison NASC (North American shale composite) from Condie (1993)

(HREE) and there is a significant Eu depletion. High field strength elements are relatively abundant including Ti (TiO_2 = 1.16 wt%), Y (45.4 ppm), Zr (197 ppm), Nb (26 ppm), and Th (21.3 ppm) (Fig. 10b). The REE and trace element diagrams show patterns similar to, but higher than those of the North Atlantic Shale Composite (NASC) indicating that the Grt-Ph schists derive from a typical shale. The TGU metasediments are unusually rich in REE in contrast to both groups of the ZSU metasediments presented and distinguished by Mahlen et al. (2005) (Fig. 10a). REE patterns from metasediments of the Valpelline series of the Dent Blanche nappe (Mahlen et al. 2005), a potential source material of the TGU Grt-Ph schists, are parallel to the TGU pattern but also contain less REE than the TGU rocks (Fig. 10a). The REE data suggest another, hitherto unknown source for the calcareous shales of the TGU.

Table 8 Average composition of granulite and eclogite facies garnet in mol% from 86 Grt analyses from Grt–Ph schist KB860. Data from Bucher et al. (2019)

G-Grt[a]	Profile 1			Profile 2		
	Average	Std.dev.	Prp max	Average	Std.dev.	Prp max
Alm	68.4	2.6	64.8	68.0	1.9	65.7
Sps	1.5	0.5	1.3	1.8	0.9	1.3
Prp	24.5	3.0	28.4	24.2	2.7	27.1
Grs	5.5	0.1	5.5	6.0	0.1	5.9
# of points	30			29		
X_{Fe}	0.74		0.70	0.74		0.71
E-Grt[b]	**Profile 1**			**Profile 2**		
	Average	Std.dev.	Grs max	Average	Std.dev.	Grs max
Alm	54.8	0.8	53.5	54.8	1.8	54.2
Sps	2.2	0.2	2.2	1.9	0.6	1.9
Prp	8.3	1.1	8.5	9.0	1.1	8.3
Grs	34.7	0.7	35.8	34.3	1.0	35.6
# of points	10			17		
X_{Fe}	0.87		0.86	0.86		0.87

[a] Granulite facies garnet

[b] Eclogite facies garnet

6.1.2 Garnet

A detailed chemical characterization of the garnets in TGU Grt-Ph schists has been presented in Bucher et al. (2019). Average compositions of granulite facies Grt cores and eclogite facies Grt rims and veins from 87 analyses are given in Table 8. The highest Prp content of typically 28 mol% Prp is found in the center of fragments of granulite facies Grt. Grossular concentration is 5.5 to 6.0 mol%.

Eclogite facies Grt between the Prp-rich fragments is rich in Grs containing up to 35.8 mol% Grs component. Pyrope with about 8.5 mol% Prp, is distinctly lower than in granulite facies fragmented cores (28%). The contact between the two Grt is very sharp and defined by the Grs content, which jumps from 6 to 35 mol% over a distance of only 2–3 µm (Bucher et al. 2019).

6.1.3 Other silicate minerals

The composition of Ph varies considerably between and within samples (Table 9). Highest measured Si is 3.4 a.p.f.u. in a Ph with low X_{Fe} but typical values are Si = 3.2 a.p.f.u. Pure Ms occurs as inclusions in Pg and as late Ms growing across the foliation. Paragonite of constant composition contains about 6 mol% Ms component. All Chl is Clc with X_{Fe} of about 0.45 for matrix Chl (Table 10). Epidote shows strong chemical zoning (Fig. 9b; Table 11). On BSE images a visible bright core indicates the presence of corroded allanite, the REE-rich variety of Ep. Some cores consist of Fe-free REE-Zo (two single point analyses on Table 11). The darker euhedral rims (BSE images, Fig. 9b) are composed of stoichiometric Ep (Clz). The two types of Amp present can be classified as Hbl and Act (Hawthorne et al. 2012), with Na of 0.75 and 0.16 a.p.f.u. respectively (Table 12). The Hbl can be characterized as ferrian subcalcic Mhb. The rim of Chl + Ab pseudomorphs after Gln (Fig. 9c) consists of Act overgrown by Hbl. Most Pl occurring in the matrix of samples KB860, OK-Z131 and OK-Z133 is oligoclase with An_{13} - An_{18}. In all samples some Ab is present particularly in pseudomorphs after Gln.

6.2 P–T model for metamorphism of the Grt-Ph schists

The following section summarizes and discusses the *P*–*T* estimates for the Grt-forming stages from Bucher et al. (2019) and presents updated *P*–*T* condition for the post-eclogite matrix assemblages.

6.2.1 Granulite facies

The cores of the porphyroblastic Grt formed at granulite facies conditions near 780 °C ± 30 and 670 MPa ± 50 (Bucher et al. 2019). The predicted assemblage at these conditions and in the presence of a graphite-controlled fluid is Grt-Kfs-Pl-Bt-Crd-Sil-Qz. Garnet with graphite inclusions (+ Qz) is the only mineral from this assemblage that survived later hydration and recrystallization.

Table 9 Composition of phengite from three samples of TGU Grt-Ph schist

	KB860				OK-Z129			OK-Z131		
	56	57	62	66	Ms1	Ms2	Ms3	Ms3	Ms4	Ms5
SiO_2	48.36	48.53	48.91	48.37	49.09	50.93	46.10	47.88	47.83	47.80
TiO_2	0.04	0.03	0.01	0.12	0.31	0.19	0.12	0.24	0.22	0.19
Al_2O_3	33.51	32.96	34.08	33.64	29.83	27.49	35.32	32.78	32.25	32.69
FeO	1.85	1.94	1.96	2.42	2.37	1.38	1.10	1.53	1.59	1.38
MgO	1.61	1.72	1.62	1.98	2.83	3.67	0.86	1.60	1.91	1.70
Na_2O	0.74	0.69	0.77	0.74	0.71	0.51	0.89	0.87	0.95	1.04
K_2O	10.27	10.47	10.27	10.27	9.98	10.19	9.59	9.82	9.92	9.73
Total	96.47	96.38	97.65	97.55	95.12	94.35	94.09	94.77	94.70	94.53
Si	3.179	3.198	3.175	3.155	3.280	3.409	3.090	3.194	3.199	3.195
Al(IV)	0.821	0.802	0.825	0.845	0.720	0.591	0.910	0.806	0.801	0.805
Al(VI)	1.776	1.757	1.782	1.741	1.630	1.577	1.879	1.771	1.741	1.770
Ti	0.002	0.001	0.000	0.006	0.015	0.010	0.006	0.012	0.011	0.010
Fe^{2+}	0.102	0.107	0.106	0.132	0.132	0.077	0.062	0.085	0.089	0.077
Mg	0.158	0.169	0.157	0.193	0.281	0.366	0.086	0.159	0.190	0.169
Na	0.094	0.088	0.097	0.094	0.091	0.066	0.115	0.112	0.123	0.134
K	0.861	0.880	0.850	0.854	0.851	0.870	0.820	0.836	0.846	0.829
X_{Fe}	0.392	0.387	0.404	0.407	0.320	0.174	0.417	0.349	0.318	0.313

Traces of Cr_2O_3, MnO and CaO (< 0.1 wt% each), mineral formulas normalized to 11 oxygen

Table 10 Composition of chlorite from four samples of TGU Grt-Ph schist

	KB 860		OK-Z129			OK-Z131		OK-Z133		
	61/1	64/1	Chl3	Chl4	Chl7	Chl-ES1	Chl-ES2	Chl-ES1	Chl1	Chl4
SiO_2	25.92	26.08	27.39	27.46	25.47	25.31	25.00	28.02	25.98	25.13
Al_2O_3	22.85	22.44	21.14	21.37	21.39	22.60	22.46	21.08	22.24	22.11
FeO	23.49	23.89	19.06	19.54	25.47	24.69	24.95	16.66	22.32	24.16
MnO	0.3	0.27	0.18	0.12	0.36	0.32	0.25	0.05	0.27	0.29
MgO	15.92	16.24	19.89	19.6	14.64	14.79	14.68	22.75	16.59	15.05
Total	88.48	88.92	87.66	88.09	87.33	87.711	87.35	88.56	87.4	86.74
Si	2.667	2.678	2.78	2.778	2.695	2.649	2.637	2.774	2.691	2.654
Al(IV)	1.333	1.322	1.22	1.222	1.305	1.351	1.363	1.226	1.309	1.346
Al(VI)	1.437	1.393	1.31	1.325	1.363	1.436	1.428	1.234	1.407	1.406
Fe^{2+}	2.021	2.051	1.618	1.653	2.254	2.161	2.200	1.379	1.933	2.134
Mn	0.026	0.023	0.016	0.01	0.033	0.028	0.023	0.004	0.024	0.026
Mg	2.442	2.486	3.01	2.956	2.309	2.308	2.308	3.358	2.562	2.370
X_{Fe}	0.45	0.45	0.35	0.36	0.49	0.48	0.49	0.29	0.43	0.47

Traces of Ti, Cr, Ca, Na and K (all < 0.1 wt%), concentrations in wt%, formulas per 14 oxygen

6.2.2 Eclogite facies

The Grs-rich second Grt generation formed at conditions of the eclogite facies, 530 °C and 1.7 GPa. The model assemblage at this *P*–*T* is Grt-Omp-Ph-Pg-Qz-Lws. The modeled assemblage differs from the observed assemblage in that neither Omp nor Lws, are present in the rock. It is possible that Omp+Lws were originally present during eclogite facies growth along a prograde subduction path, but were later removed from the matrix during complete greenschist facies recrystallization of the rock matrix. The model fails to predict the presence of glaucophane at the eclogite stage or pre-eclogite stage for which there is textural evidence in the form of Ab-Chl pseudomorphs (Fig. 9c) produced by the reaction 1:

$$1\,\mathrm{Gln} + 1\,\mathrm{Pg} + 1\,\mathrm{Qz} + 2\,\mathrm{H_2O} = 1\,\mathrm{Chl} + 3\,\mathrm{Ab} \quad (1)$$

Table 11 Composition of epidote/clinozoisite/allanite from three samples of TGU Grt-Ph schist

	KB860			OK-Z131		OK-Z133			
	Epidote	Allanite	REE-Zoisite	Ep1	Ep2	Ep-ES1	Ep1	Ep2	Ep3
SiO_2	37.05	34.42	34.30	38.51	38.81	38.88	39.39	39.55	39.13
Al_2O_3	30.43	27.26	26.24	28.13	28.79	30.66	32.65	32.60	32.35
Fe_2O_3	4.92	4.92		5.75	5.44	4.41	1.48	1.76	1.91
MnO	0.11	0.01	0.03	0.10	0.10	0.16	0.00	0.07	0.00
MgO	0.04	0.31	0.15	0.03	0.00	0.00	0.00	0.00	0.00
CaO	23.60	21.49	21.54	22.96	23.94	23.97	24.53	24.69	24.21
Total	96.15	88.41	82.26	95.48	97.08	98.08	98.05	98.67	97.60
Si	2.91	2.85	2.97	3.03	3.01	2.97	2.99	2.98	2.98
Al	2.82	2.66	2.68	2.61	2.63	2.76	2.92	2.90	2.91
Fe^{3+}	0.29	0.34		0.38	0.35	0.28	0.09	0.11	0.12
Ca	1.99	1.91	2.00	1.93	1.99	1.96	1.99	2.00	1.98

Epidote rim = Euhedral overgrowth on corroded REE-rich allanite (core). REE-zoisite = Fe-free zoisite containing about 15 wt% REE_2O_3 total

Formulas normalized to 12.5 oxygen

Table 12 Composition of amphibole from two samples of TGU Grt-Ph schist

	KB860		OK-Z129		OK-Z129	
	Hornblende	Hornblende	Actinolite	Actinolite	Hornblende	Hornblende
Point	76	77	4	5	2	3
SiO_2	48.37	48.76	55.04	54.86	49.20	48.43
TiO_2	0.07	0.04	0.03	0.06	0.07	0.12
Al_2O_3	11.29	11.96	3.74	3.29	11.07	12.28
FeO	13.38	13.17	7.82	8.75	13.71	13.49
MnO	0.17	0.12	0.13	0.14	0.14	0.35
MgO	12.73	12.22	18.69	18.24	12.40	11.78
CaO	9.05	8.71	12.35	12.38	8.86	8.99
Na_2O	2.16	2.57	0.60	0.46	2.67	2.35
K_2O	0.23	0.15	0.07	0.06	0.19	0.34
Total	97.45	97.7	98.45	98.24	98.32	98.12
Si	6.995	7.010	7.668	7.694	7.057	6.961
Al^{IV}	1.005	0.990	0.332	0.306	0.943	1.039
Al^{VI}	0.919	1.037	0.282	0.237	0.929	1.041
Ti	0.008	0.004	0.003	0.006	0.007	0.013
Fe	1.618	1.583	0.911	1.026	1.645	1.622
Mn	0.021	0.015	0.015	0.017	0.017	0.043
Mg	2.744	2.619	3.881	3.813	2.652	2.525
Ca	1.402	1.342	1.843	1.860	1.362	1.385
Na	0.606	0.716	0.161	0.124	0.744	0.655
K	0.042	0.028	0.012	0.010	0.035	0.062
X_{Fe}	0.37	0.38	0.19	0.21	0.38	0.39

Formula based on 23 oxygen

6.2.3 First greenschist facies event

The assemblage Chl-Ab-Pg-Ms-Act-Qz is characteristic of greenschist facies conditions. The textures suggest that the greenschist facies overprint followed the eclogite facies. The P–T conditions of this stage probably where close to 350 °C and 300 MPa (Bucher et al. 2019).

6.2.4 Second greenschist facies recrystallization

In the recrystallized matrix of the schists, Pl with An_{18} and Cam with Prg_{70} record prograde metamorphism up to the greenschist to amphibolite facies boundary. The Ep/Clz of the matrix belongs to the same assemblage together with both white micas and Qz. A *P*–*T* estimate of 470 °C and 650 MPa for this last and prograde metamorphic stage results from new Theriak models using the matrix composition given in Bucher et al. (2019). The model reproduces the observed Pl and Cam composition and the matrix assemblage. This metamorphic stage has not been modeled previously and the derived *P*–*T* estimate is comparable to the *P*–*T* estimate of 550 MPa and 450 °C derived for the SW9 metabasalt given above. The metamorphic stage most likeley reflects the effect of the late Alpine collision phase.

7 Interpretation and discussion of data

7.1 Variscan granulite facies metamorphism

The composition of the cores of porphyroblastic Grt is evidence for granulite facies metamorphism of the metasediments of the TGU. The morphology of Zrn in mafic metavolcanic rocks of the TGU is consistent with a metamorphic granulite facies origin. The upper intercept age at 295 ± 16 Ma (Fig. 8) suggests that the high-grade metamorphism occurred close to the Carboniferous–Permian boundary in the final stages of the Variscan orogeny. High-grade metamorphic metapelites have been reported from the Valpelline Series within the Dent Blanche nappe, the tectonically highest unit of the Zermatt region (Figs. 1 and 2) (Nicot 1977; Gardien et al. 1994; Bucher et al. 2004; Manzotti and Zucali 2013; Manzotti et al. 2014). These rocks carry the assemblage Grt-Pl-Kfs-Qz-Bt-Sil, locally also Crd (Diehl et al. 1952; Bucher et al. 2004; Zucali et al. 2011). The assemblage is identical to the predicted stable assemblage for the Grt core generation in the TGU Grt-Ph schists. Manzotti and Zucali (2013) reported peak metamorphic conditions of 814 ± 40 °C and 600–800 MPa for samples of the Valpelline Series that were then subsequently dated by Kunz et al. (2018). That geochronologic study yielded a Permian age, 280 ± 20 Ma overlapping with our SW9 zircon age within the given errors. The published *P*–*T* conditions for the Dent Blanche granulites are identical with the derived conditions of garnet growth for the TGU sample (780 °C ± 30 and 670 MPa ± 50). The high-grade metamorphism in Dent Blanche granulites was related to regional lithospheric thinning during the late Paleozoic (Kunz et al. 2018; Manzotti et al. 2018).

7.2 Origin of the TGU and possible involvement in Jurassic extensional processes

The similarities of the TGU rocks with the high-grade metasediments of the Valpelline unit of the overriding Dent Blanche nappe described above may indicate that the TGU represents material from the Dent Blanche nappe in spite of not perfectly matching REE patterns (Fig. 10a). How the material crossed the basal thrust and the underlying units to end up as an isolated slab in the ZSU remains unknown. An process of subduction erosion has been proposed for the Allalin gabbro within the Zermatt-Saas ophiolites (Bucher and Grapes 2009). Alternatively, the TGU slab could represent a relic of an extensional allochton, similar to slices of continental basement occurring further south in the ZSU (Beltrando et al. 2010). The slab may have been incorporated into the newly forming oceanic lithosphere during the early stages of continental rifting and extension in Mid-Jurassic time. However, the TGU slab has not been intruded by oceanic basic melts, gabbros and basalts of the ZSU. All contacts between the TGU and ZSU are strictly tectonic, in support of a tectonic process related to either the subduction or collision phase of the alpine orogeny. On the other hand, the granulite facies Zrn from eclogite SW9 indicate that they have been modified by an event, probably the continental breakup, at the Jurassic–Cretaceous boundary (lower intercept age of 145 ± 34 Ma). It is difficult to weight the indications for extensional allochton versus subduction erosion unequivocally.

7.3 Alpine eclogite facies metamorphism and relations between TGU and ZSU

Eclogite facies metamorphism has been recorded by both the meta-volcanic rocks and the metasediments. The mafic rock SW9 yielded 503 °C and 1.63 GPa whilst the Grt-Ph schist KB860 supplied 530 °C and 1.7 GPa for the eclogite facies conditions related to Alpine subduction. The 1.63 GPa maximum pressure corresponds to 55 km depth and the temperature of 520 °C gives a geothermal gradient of about 9.5 °C km^{-1} (for a rock density of 3000 kg m^{-3}). The peak conditions of the eclogite facies metamorphism has been dated by Lu–Hf garnet-whole rock isochrons of 56.5 ± 2.7 Ma for the TGU eclogite SW9 and 58.2 ± 1.4 Ma for another sample SW14 (Weber et al. 2015).

Note that Weber and Bucher (2015) reported *P*–*T* conditions of 580 °C and 2.2 GPa for the TGU eclogites and interpreted them as peak conditions of subduction metamorphism. However, the coincidence of our new *P*–*T* conditions derived for eclogite SW9 and Grt-Ph schist KB860 suggests that the peak conditions are lower than previously reported. It remains a possibility though that

the TGU does not represent a coherent unit. The field occurrence of some of the eclogites as boudins, lenses and rotated blocks in the Grt-Ph schists (Fig. 5a, b) suggests that they have been tectonically emplaced in the schists. Thus there may occur two types of eclogites in the TGU: (i) one with a maximum *P* of 1.63 GPa identical to the *P* of eclogite facies Grt formation in the Grt-Ph schists and (ii) one type with maximum P significantly higher (up to 2.2 GPa). The most likely solution resolving the inconsistency is, however, that the eclogite sample providing the 2.2 GPa pressure (LX15 in Weber and Bucher 2015) is a tectonically emplaced fragment from the ZSU (see *P*–*T* estimates below).

The maximum pressure recorded by the assemblages of the Zermatt-Saas meta-ophiolites range from 2.2 to 2.4 GPa (Angiboust et al. 2009) for eclogites of the area near Zermatt, from 2.5 to 2.7 GPa (Bucher et al. 2005) near the Pfulwe locality (Fig. 1) and 2.5 GPa for the eclogite facies Allalin gabbro (Fig. 1) (Bucher and Grapes 2009). The large range of derived pressures may indicate that several separate slices with different subduction - exhumation paths are present within the high-pressure meta-ophiolites. *P*–*T* conditions of 2.3 - 2.4 GPa and 500 ± 50 °C have been reported for eclogites belonging to the ZSU of the Trockener Steg area enveloping the TGU with its Grt-Ph schists (Weber and Bucher 2015). This maximum pressure of 2.3–2.4 GPa is consistent with the estimates cited above and well within the uncertainty of the applied methods for estimating the pressures. This maximum pressure corresponds to a depth of 80–85 km for the return-point at which the ZSU ophiolites detached from the subducting slab and began the ascent to the shallow crust. At the locality Lago di Cignana (LdC on Fig. 1) about 30 km south of Trockener Steg, Coe has been reported from rocks that may belong to the ZSU (Reinecke 1991). This may indicate that some parts of the ZSU ophiolites have been subducted to more than 90 km depth. A similar return-point has also been suggested for the Pfulwe locality (Fig. 1) on the basis of the stable Cld-Tlc assemblage found in eclogite facies glaucophanites from this locality (Bucher et al. 2005). Estimated maximum temperatures at the return-point range from 520 to 600 °C and by and large correlate with the derived pressures suggesting a coherent subduction geotherm of about 8 ± 1 °C km^{-1} (Bucher et al. 2005; Angiboust et al. 2009; Bucher and Grapes 2009; Groppo et al. 2009; Rebay et al. 2012).

Lu–Hf garnet whole-rock ages of 56.5 ± 2.7 and 58.2 ± 1.4 Ma for two TGU eclogite samples including SW9 indicate that eclogite facies metamorphism of the TGU occurred in the Palaeocene (Weber et al. 2015). The late Paleocene subduction age from the TGU eclogites is considerably older than the Mid-Eocene Rb–Sr phengite ages of 43 - 46 Ma from the ZSU meta-ophiolites (Dal Piaz et al. 2001). Sm–Nd and Lu–Hf geochronology on the ZSU indicate protracted garnet growth during prograde metamorphism and showed that the ZSU underwent peak metamorphic HP conditions less than 43 m.y. ago (de Meyer et al. 2014). The ZSU rocks reached greenschist-facies conditions around 38 ± 2 Ma on the basis of Rb–Sr whole rock–phengite isochrons (Amato et al. 1999). A Mid-Eocene age of 44.1 ± 0.7 Ma was also derived from whole Zrn and Zrn rims in eclogite at Lago di Cignana by Rubatto et al. (1998), confirming Sm–Nd isotopic analyses of an essentially unretrogressed eclogitic metabasalt suggest that eclogite facies metamorphism occurred at 52 ± 18 Ma. The large uncertainty is due to the presence of very small amounts of Nd- rich epidote present as inclusions within garnet (Bowtell et al. 1994).

The age difference for the eclogite facies metamorphism between the TGU and ZSU can be related to the northwards progressing subduction process. Subduction ages in the range of 55 to 77 Ma have been reported for eclogite facies rocks of the Sesia Unit south of the Zermatt region and tectonically above the ZSU (Giuntoli et al. 2018). Thus deformation and metamorphism migrated from internal to external parts, that is, mostly towards northwest (e.g. Handy et al. 2010). It is not clear to what extent this migration was continuous or episodic (Lister et al. 2001). It implies that the TGU slab was not subducted together with the meta-ophiolites of the ZSU but reached its position within the ZSU (Fig. 3) later probably during late thrusting of the nappe stack.

7.4 Final metamorphism during exhumation and nappe emplacement

The first greenschist facies recrystallization replacing e.g. Gln by Chl-Ab pseudomorphs at 350 °C and 300 MPa concludes the subduction related exhumation path. The *P*–*T* conditions of 470 °C, 650 MPa for the second matrix recrystallization can been placed on the derived exhumation path for units in the Zermatt area (Weber and Bucher 2015). However, this late prograde matrix recrystallization could also be related to deformation overprinting the high-pressure rocks during Alpine nappe stacking. The derived *P*–*T* conditions of the matrix recrystallization correspond the conditions for late Alpine greenschist to lower amphibolite facies overprint recorded by the rocks of the ophiolite nappe Zermatt-Saas (Bearth 1967; Barnicoat et al. 1995; Bucher et al. 2005; Bucher and Grapes 2009; Angiboust et al. 2009). Thus the preferred interpretation of the latest assemblage oligoclase + magnesio-hornblende is that it formed by prograde metamorphism related to the latest deformation of thrusting and backfolding in the late Eocene (e.g.

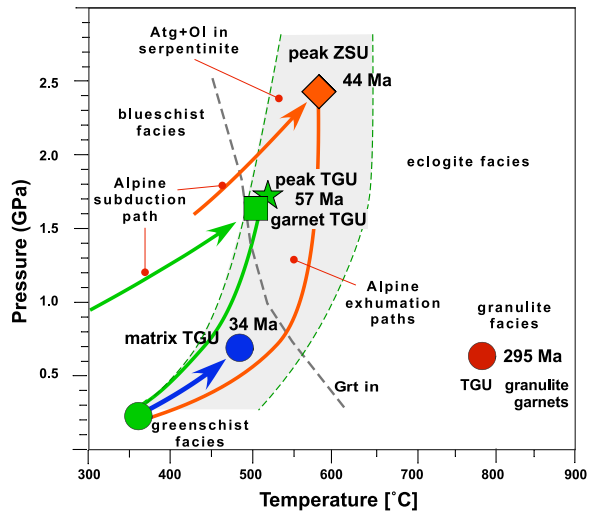

Fig. 11 Summary of metamorphic conditions and ages: Prealpine granulite facies metamorphism at 295 Ma (red point). Alpine subduction related high-P low-T metamorphism: Garnet in TGU at 57 Ma: Peak *P–T* conditions reached by the TGU (green symbols) and the ZSU (orange symbols) in the Zermatt area (average from Bucher et al. 2005; Angiboust et al. 2009; Bucher and Grapes 2009; age from Rubatto et al. 1998). Possible prograde paths for alpine subduction metamorphism and subsequent exhumation is constrained by the presence of stable Ol + Atg in the ZSU serpentinites (Li et al. 2004a). Exhumation of TGU and ZSU terminated at greenschist facies conditions (green circle). The conditions calculated for the matrix recrystallization of the TGU were reached along a prograde path (blue symbols) starting at the exhumation path and attaining the *P–T* maximum for this event not later than 34 Ma ago (Amato et al. 1999). The final exhumation path of both units is not shown

Dent Blanche nappe thrust above Eocene of the Barrhorn Series, Ellenberger 1953).

8 Conclusions

The geological history of the TGU outlined above is summarized on Fig. 11. Both the metamorphic igneous and sedimentary rocks of the TGU experienced granulite facies metamorphism 295 Ma ago at the Carboniferous–Permian boundary in the context of the last stages of the Variscan orogeny (red circle Fig. 11). The granulite facies zircons from eclogite SW9 indicate that they have been modified by an event at the Jurassic–Cretaceous boundary (not shown on Fig. 11). This may have been the transformation of the TGU to an extensional allochton. In any case the zircon U–Pb systems were further disturbed during the Alpine subduction events (green symbols on Fig. 11).

Lu–Hf garnet-whole rock analyses show that subduction of the TGU occurred in the Paleocene about 57 Ma ago (Weber et al. 2015) earlier than the main subduction of the ZS meta-ophiolites at 43 Ma in the Mid-Eocene (Rubatto et al. 1998; de Meyer et al. 2014). The Zrn data presented here have been extracted from Zrn in the same sample SW9 that also supplied the Lu–Hf garnet-whole rock ages making us confident that the Permian, Jurassic and Paleogene ages depict a consistent geological history.

New *P–T* estimates for both eclogites and metasediments suggest that the TGU reached about 53 km depth during subduction in contrast to 90 km of the ZSU.

During exhumation, the high-pressure assemblages of the TGU rocks were retrogressed to greenschist facies assemblages at conditions as low as 350 °C and 300 MPa (green circle Fig. 11). There is evidence in the Grt-Ph schists of a prograde recrystallization of the matrix at significantly higher *P–T* of 650 MPa and 470 °C (blue symbols Fig. 11). This latest metamorphic overprint has also been reported from eclogites of the ZSU near Trockener Steg (Fig. 3) with a *P–T* estimate of 750 MPa and 496 °C for the late event (Angiboust et al. 2009). It is plausible that the large scale thrusting and folding that formed the present day geometry of the nappe stack occurred after the exhumation of the high-pressure rocks. The pressure increase of 450 MPa associated with this late deformation corresponds to a burial of TGU and ZSU by about 15 km, leading to the temperature increase of 130 °C.

The ZSU reached its greatest subduction depth at 44 Ma that is in the Mid-Eocene (Rubatto et al. 1998; de Meyer et al. 2014) and the Dent Blanche nappe (Figs. 1 and 2) was thrusted over Eocene sediments at the Barrhorn (Ellenberger 1953). The Eocene ends at 34 Ma (Gradstein et al. 2004). The proposed age limits are consistent with those given in Steck et al. (2015). This leaves a maximum of 10 Ma for exhuming the high-pressure rocks from 90 km depth to the shallow crust at 300 MPa (10 km) and subsequent large scale deformation including the formation of the nappe stack, the Mittaghorn fold controlling the geometry of the meta-ophiolite nappe ZSU and the Mischabel backfold with which the late overprint at the greenschist to amphibolite facies transition of the TGU is associated with (Fig. 11). Using 50% of this time for exhumation after peak pressure results in a vertical exhumation rate of 16 mm a^{-1}. This conclusion is consistent with the evidence for unusually high exhumation rates for the ZSU of 10–26 mm a^{-1} reported by Amato et al. (1999).

Acknowledgements

We are grateful for rock composition data provided by Isolde Schmidt and microprobe operation by Hiltrud Müller-Sigmund. We thank Ingrid Stober and Zhou Wei for help with the fieldwork. The suggestions and comments from two constructive reviews are gratefully acknowledged. We thank Edwin Gnos for his thoughtful editorial work.

Authors' contributions

KB carried out field work, thin section examination, microprobe work, phase equilibrium computation and drafted the figures and the manuscript. TBW has been involved in an earlier version of the paper and provided feedback to the present manuscript. SW carried out fieldwork and provided composition

data of the TGU eclogite SW9. OK carried out field work and provided data from the OK samples. FC performed the U/Pb dating of the zircons from the TGU eclogite. All co-authors provided feedback to earlier drafts and read and approved the final manuscript.

Competing interests
The authors declare that they have no competing interests.

Author details
[1] Mineralogy & Petrology, University of Freiburg, Albertstr. 23b, 79104 Freiburg, Germany. [2] Iceland GeoSurvey (ÍSOR), Grensásvegur 9, 108 Reykjavík, Iceland. [3] Sächsisches Landesamt für Umwelt, Landwirtschaft und Geologie, Referat 102, Halsbrücker Str.31a, 09599 Freiberg, Germany. [4] Im Laimacker 41, 79249 Merzhausen, Germany. [5] Department of Geosciences and CEED, University of Oslo, Postboks 1047, Blindern, 0316 Oslo, Norway.

Received: 3 July 2019 Accepted: 18 November 2019
Published online: 17 February 2020

References

Amato, J. M., Baumgartner, L., Johnson, C. M., & Beard, M. (1999). Rapid exhumation of the Zermatt-Saas ophiolite deduced from high-pressure Sm-Nd and Rb-Sr geochronology. *Earth and Planetary Science Letters, 171,* 425–438.

Angiboust, S., Agard, P., Jolivet, L., & Beyssac, O. (2009). The Zermatt-Saas ophiolite: the largest (60-km wide) and deepest (c. 70–80 km) continuous slice of oceanic lithosphere detached from a subduction zone? *Terra Nova, 21,* 171–180.

Argand, E. (1908). Carte géologique du massif de la Dent Blanche, 1:50000: Schweiz. geol. Komm.

Argand, E. (1911). Les nappes de recouvrement des Alpes Pennines et leurs prolongements structuraux. *Beiträge zur Geologischen Karte der Schweiz, 31,* 1–26.

Ballèvre, M., Kienast, J. R., & Vuichard, J. P. (1986). La nappe de la Dent Blanche (Alpes occidentales): Deux unités austroalpines indépendentes. *Eclogae Geologicae Helvetiae, 79,* 57–74.

Barnicoat, A. C., & Fry, N. (1986). High-pressure metamorphism of the Zermatt-Saas ophiolite zone, Switzerland. *Journal of the Geological Society of London, 143,* 607–618.

Barnicoat, A. C., Rex, D. C., Guise, P. G., & Cliff, R. A. (1995). The timing of and nature of green schist facies deformation and metamorphism in the upper Pennine Alps. *Tectonics*, *14*, 279–293.

Bearth, P. (1967). Die Ophiolithe der Zone von Zermatt-Saas Fee. *Beiträge zur geologischen Karte der Schweiz, N.F. 132*, p. 130.

Bearth, P., & Schwander, H. (1981). The post-Triassic sediments of the ophiolite zone Zermatt-Saas Fee and the associated manganese mineralizations. *Eclogae Geologicae Helvetiae, 74,* 189–205.

Beltrando, M., Rubatto, D., & Manatschal, G. (2010). From passive margins to orogens: The link between ocean-continent transition zones and (ultra) high-pressure metamorphism. *Geology, 38,* 559–562.

Berman, R. B. (1988). Internally consistent thermodynamic data for minerals in system: Na2O–K2O–CaO–MgO–FeO–Fe2O3–Al2O3–SiO2–TiO2–H2O–CO2. *Journal of Petrology, 29,* 445–522.

Bowtell, S. A., Cliff, R. A., & Barnicoat, A. C. (1994). Sm–Nd isotopic evidence on the age of eclogitization in the Zermatt-Sass ophiolite. *Journal of Metamorphic Geology, 12,* 187–196.

Bucher, K., Dal Piaz, G. V., Oberhänsli, R., Gouffon, Y., Martinotti, G., & Polino, R. (2003). Blatt 1347 Matterhorn. *Geol. Atlas Schweiz 1:25000, Karte 107*.

Bucher, K., Dal Piaz, G. V., Oberhänsli, R., Gouffon, Y., Martinotti, G., & Polino, R. (2004). Blatt 1347 Matterhorn. *Geol. Atlas Schweiz 1:25000, Erläuterungen 107,* p. 73.

Bucher, K., Fazis, Y., de Capitani, C., & Grapes, R. (2005). Blueschists, eclogites and decompression assemblages of the Zermatt-Saas ophiolite: high-pressure metamorphism of subducted Tethys lithosphere. *American Mineralogist, 90,* 821–835.

Bucher, K., & Grapes, R. (2009). The Eclogite-facies Allalin Gabbro of the Zermatt-Saas Ophiolite, Western Alps: a Record of Subduction Zone Hydration. *Journal of Petrology, 50,* 1405–1442.

Bucher, K., Weisenberger, T., Weber, S., & Klemm, O. (2019). Decoding the complex internal chemical structure of garnet porphyroblasts from the Zermatt area, Western Alps. *Journal of metamorphic Geology 37,* 1151–1169. https://doi.org/10.1111/jmg.12506.

Condie, K. C. (1993). Chemical composition and evolution of the upper continental crust: contrasting results from surface samples and shales. *Chemical Geology, 104,* 1–37.

Corfu, F. (2004). U-Pb age, setting, and tectonic significance of the anorthosite-mangerite charnockite-granite-suite, Lofoten-Vesterålen, Norway. *Journal of Petrology, 45,* 1799–1819.

Dal Piaz, G. V., Bistacchi, A., Gianotti, F., Monopoli, B., & Passeri, L. (2015). Note illustrative della carta Geologica d'Italia alla scala 1:50000. Foglio 070, Cervino. *Servizio Geologico d'Italia, 070,* 1–431.

Dal Piaz, G. V., Cortiana, G., Del Moro, A., Martin, S., Pennacchioni, G., & Tartarotti, P. (2001). Tertiary age and paleostructural inferences of the eclogitic imprint in the Austroalpine outliers and Zermatt-Saas ophiolite, western Alps. *International Journal of Earth Sciences, 90,* 668–684.

Dal Piaz, G. V., De Vecchi, G., & Hunziker, J. (1977). The Austroalpine layered gabbros of the Matterhorn and Mont Collon - Dents de Bertol. *Schweizerische Mineralogische und Petrographische Mitteilungen, 57,* 59–81.

de Capitani, C., & Petrakakis, K. (2010). The computation of equilibrium assemblage diagrams with Theriak/Domino software. *American Mineralogist, 95,* 1006–1016.

de Meyer, C. M. C., Baumgartner, L. P., Beard, B. L., & Johnson, C. M. (2014). Rb–Sr ages from phengite inclusions in garnets from high pressure rocks of the Swiss Western Alps. *Earth and Planetary Science Letters, 395,* 205–216.

Diehl, E. A., Masson, R., & Stutz, A. H. (1952). Contributo alla conoscenza del ricoprimento della Dent Blanche. *Memorie degli Istituti di Geologia e Mineralogia dell'Università di Padova, 17,* 1–52.

Ellenberger, F. (1953). La série du Barrhorn et les rétrocharriages penniques: *C. R. Acad. Sci. (Paris), 236,* 218–220.

Escher, A., Masson, H., & Steck, A. (1993). Nappe geometry in the Western Swiss Alps. *Journal of Structural Geology, 15,* 501–509.

Fassmer, K., Obermüller, G., Nagel, T. J., Kirst, F., Froitzheim, N., Sandmann, S., et al. (2016). High-pressure metamorphic age and significance of eclogite-facies continental fragments associated with oceanic lithosphere in the Western Alps (Etirol-Levaz Slice, Valtournenche, Italy. *Lithos, 252–253,* 145–159.

Ganguin, J. (1988). *Contribution à la caractérisation du métamorphisme polyphases de la zone de Zermatt-Saas Fee (Alps Valaisannes)* (p. 312). Unpub PhD, ETH, Zürich: Switzerland.

Gardien, V., Reusser, E., & Marquer, D. (1994). Pre-Alpine metamorphic evolution of the gneisses from the Valpelline series (Western Alps, Italy). *Schweizerische Mineralogische und Petrographische Mitteilungen, 74,* 489–502.

Giuntoli, F., Lanari, P., Burn, M., Kunz, B. E., & Engi, M. (2018). Deeply subducted continental fragments – Part 2: Insight from petrochronology in the central Sesia Zone (western Italian Alps). *Solid Earth*, *9*, 191–222.

Gosso, G., Dal Piaz, G.V., Piovano, V. & Polino, R. (1979). High pressure implacement of early-alpine nappes, postnappe deformations and structural levels. Memorie della Societa` Geologica Italiana, 32, p 15.

Gradstein, F., Ogg, J., Smith, A., et al. (2004). A Geologic Time Scale 2004. *Cambridge University Press,* 589 p.

Gromet, L. P., Haskin, L. A., Korotev, R. L., & Dymek, R. F. (1984). The "North American shale composite": its compilation, major and trace element characteristics. *Geochimica et Cosmochimica Acta, 48,* 2469–2482.

Groppo, C., Beltrando, M., & Compagnoni, R. (2009). The P-T path of the ultra-high pressure Lago di Cignana and adjoining high-pressure meta-ophiolitic units: insights into the evolution of the subducting Tethyan slab. *Journal of Metamorphic Geology, 27,* 207–231.

Handy, M. R., Schmid, S. M., Bousquet, R., Kissling, E., & Bernoulli, D. (2010). Reconciling plate-tectonic reconstructions of Alpine Tethys with the geological–geophysical record of spreading and subduction in the Alps. *Earth-Science Reviews, 102,* 121–158.

Hawthorne, F. C., Oberti, R., Harlow, G. E., Maresch, W. V., Martin, R. F., Schumacher, J. C., et al. (2012). Nomenclature of the amphibole supergroup. *American Mineralogist, 97,* 2031–2048.

Jaffey, A. H., Flynn, K. F., Glendenin, L. E., Bentley, W. C., & Essling, A. M. (1971). Precision measurement of half–lives and specific activities of ^{235}U and ^{238}U. *Physical Review, Section C, Nuclear Physics, 4,* 1889–1906.

Keller, J. M., de Capitani, C., & Abart, R. (2005). A quaternary solution model for white micas based on natural coexisting phengite–paragonite pairs. *Journal of Petrology, 46,* 2129–2144.

Klemm, O. (2005). Die metamorphe Entwicklung der metabasischen und metasedimentären Anteile der Zermatter Ophiolithe im Bereich Lichenbretter - Oberer Theodulgletscher, Wallis, Schweiz. *Unpublished MSc thesis (Diplomarbeit), University of Freiburg, Germany*, p. 115.

Konrad-Schmolke, M., Zack, T., O'Brien, P. J., & Jacob, D. E. (2008). Combined thermodynamic and rare earth element modeling of garnet growth during subduction: examples from ultrahigh-pressure eclogite of the Western Gneiss Region, Norway. *Earth and Planetary Science Letters, 272,* 488–498.

Krogh, T. E. (1973). A low-contamination method for hydrothermal decomposition of zircon and extraction of U and Pb for isotopic age determinations. *Geochimica et Cosmochimica Acta, 37,* 485–494.

Kunz, B. E., Manzotti, P., von Niederhäusern, B., Engi, M., Darling, J. R., Giuntoli, F., et al. (2018). Permian high-temperature metamorphism in the Western Alps (NW Italy). *International Journal of Earth Sciences, 107,* 203–229.

Lapen, T. J., Johnson, C. M., Baumgartner, L. P., Mahlen, N. J., Beard, B. L., & Amato, J. M. (2003). Burial rates during prograde metamorphism of an ultra-high-pressure terrane: an example from Lago di Cignana, western Alps, Italy. *Earth and Planetary Science Letters, 215,* 57–72.

Li, X.-P., Rahn, M., & Bucher, K. (2004a). Serpentinites of the Zermatt-Saas ophoilite complex and their texture evolution. *Journal of Metamorphic Geology, 22,* 159–178.

Li, X.-P., Rahn, M., & Bucher, K. (2004b). Metamorphic Processes in Rodingites of the Zermatt-Saas Ophiolites. *International Geology Review, 46,* 28–51.

Li, X.-P., Rahn, M., & Bucher, K. (2008). Eclogite-facies metarodingites: phase relations in the system SiO_2–Al_2O_3–FeO–Fe_2O_3–MgO–CaO–CO_2–H_2O; an example from the Zermatt-Saas Ophiolite. *Journal of Metamorphic Geology, 26,* 347–364.

Lister, G. S., Forster, M. A., & Rawling, T. J. (2001). Episodicity during orogenesis. In J. A. Miller, R. E. Holdsworth, I. S. Buick, & M. Hand (Eds.), *Continental Reactivation and Reworking* (pp. 89–113). London: Geological Society London: Special Publications.

Ludwig, K. R. (2009). *Isoplot 41 A geochronological toolkit for Microsoft Excel*. Berkeley: Berkeley Geochronology Center Special Publication.

Mahlen, N. J., Johnson, C. M., Baumgartner, L. P., & Beard, B. L. (2005). Provenance of Jurassic Tethyan sediments in the HP/UHP Zermatt-Saas ophiolite, western Alps. *GSA Bulletin, 117,* 530–544.

Manzotti, P., Ballèvre, M., & Dal Piaz, G. C. (2017). Continental gabbros in the Dent Blanche Tectonic System (Western Alps): from the pre-Alpine crustal structure of the Adriatic palaeo-margin to the geometry of an alleged subduction interface. *Journal of the Geological Society, 174,* 541–556.

Manzotti, P., Ballèvre, M. Z., Robyr, M., & Engi, M. (2014). The tectonometamorphic evolution of the Sesia-Dent Blanche nappes (internal Western Alps): review and synthesis. *Swiss Journal of Geosciences, 107,* 309–336.

Manzotti, P., Rubatto, D., Zucali, M., El Korh, A., Cenki-Tok, B., Ballèvre, M., et al. (2018). Permian magmatism and metamorphism in the Dent Blanche nappe: constraints from field observations and geochronology. *Swiss Journal of Geosciences, 111,* 79–97.

Manzotti, P., & Zucali, M. (2013). The pre-Alpine tectonic history of the Austroalpine continental basement in the Valpelline unit (Western Italian Alps). *Geological Magazine, 150,* 153–172.

Mattinson, J. M. (2005). Zircon U-Pb chemical abrasion ('CA-TIMS') method: Combined annealing and multi-step partial dissolution analysis for improved precision and accuracy of zircon ages. *Chemical Geology, 220,* 47–66.

McDonough, W. F., & Sun, S. S. (1995). The composition of the Earth. *Chemical Geology, 120,* 223–253.

Meyre, C., de Capitani, C., & Partzsch, J. H. (1997). A ternary solid solution model for omphacite and its application to geothermobarometry of eclogites from the Middle Adula nappe (Central Alps, Switzerland). *Journal of Metamorphic Geology, 15,* 687–700.

Nicot, E. (1977). Les Roches mew ct catazonales de la Valpelline (Nappe de la Dent Blanche, Alpes Italiennes). *Thèse 3ème cycle. Paris VI.*, p. 325.

Piaz, G.V. (1965). La formazione mesozoica dei calcescisti con pietre verdi fra la Valsesia e la Valtournanche ed i suoi rapporti con il ricoprimento Monte Rosa e con la Zona Sesia-Lanzo. *Bull Soc Geol ital, 84*, 67–104.

Rebay, G., Spalla, M. I., & Zanoni, D. (2012). Interaction of deformation and metamorphism during subduction and exhumation of hydrated oceanic mantle: isights from the Western Alps. *Jounal of metamorphic Geology, 30,* 687–702.

Reinecke, T. (1991). Very-high-pressure metamorphism and uplift of coesite-bearing metasediments from the Zermatt-Saas zone, Western Alps. *European Journal of Mineralogy, 3,* 7–17.

Reinecke, T. (1998). Prograde high- to ultrahigh-pressure metamorphism and exhumation of oceanic sediments at Lago di Cignana, Zermatt-Saas Zone, western Alps. *Lithos, 42,* 147–189.

Rubatto, D., Gebauer, D., & Fanning, M. (1998). Jurassic formation and Eocene subduction of the Zermatt-Saas-Fee ophiolites: implications for the geodynamic evolution of the Central and Western Alps. *Contributions to Mineralogy and Petrology, 132,* 269–287.

Rubatto, D., & Hermann, J. (2003). Zircon formation during fluid circulation in eclogites (Monviso, Western Alps): Implications for Zr and Hf budget in subduction zones. *Geochimica et Cosmochimica Acta, 67,* 2173–2187.

Rudnick, R. L., & Gao, S. (2003). Composition of the Continental Crust. In H. D. Holland & K. K. Turekian (Eds.), *Treatise on Geochemistry* (pp. 1–64). Oxford: Pergamon.

Skora, S., Mahlen, N. J., Johnson, C. M., Baumgartner, L. P., Lapen, T. J., Beard, B. L., et al. (2015). Evidence for protracted prograde metamorphism followed by rapid exhumation of the Zermatt-Saas Fee ophiolite. *Journal of Metamorphic Geology, 33,* 711–734.

Stacey, J. S., & Kramers, J. D. (1975). Approximation of terrestrial lead isotope evolution by a two-stage model. *Earth and Planetary Science Letters, 34,* 207–226.

Steck, W., Masson, H., & Robyr, M. (2015). Tectonics of the Monte Rosa and surrounding nappes (Switzerland and Italy): Tertiary phases of subduction, thrusting and folding in the Pennine Alps. *Swiss Journal of Geosciences, 108,* 3–34.

Weber, S., & Bucher, K. (2015). An eclogite-bearing continental tectonic slice in the Zermatt-Saas high-pressure ophiolites at Trockener Steg (Zermatt, Swiss Western Alps). *Lithos, 232,* 336–359.

Weber, S., Sandmann, S., Miladinova, I., Fonseca, R. O. C., Froitzheim, N., Münker, C., et al. (2015). Dating the Initiation of Piemonte-Liguria Ocean Subduction: Lu–Hf Garnet Chronometry of Eclogites From the Theodul Glacier Unit (Zermatt–Saas Zone, Switzerland). *Swiss Journal of Geosciences, 108,* 183–199.

Whitney, D. L., & Evans, B. W. (2010). Abbreviations for names of rock-forming minerals. *American Mineralogist, 95,* 185–187.

Zucali, M., Manzotti, P., Diella, V., Pesenti, C., Rispendente, A., Darling, J., et al. (2011). Permian tectonometamorphic evolution of the Dent-Blanche Unit (Austroalpine domain, Western Italian Alps). *Rendiconti online Soc. Geol. It., 15,* 133–136.

Publisher's Note